An International Journal of Optimization and Control: Theories & Applications
ISSN: 2146-0957 eISSN: 2146-5703
Vol.16, No.6, pp.2171-2193 (2026)
https://doi.org/10.36922/IJOCTA026280155

RESEARCH ARTICLE

Robust fixed-time sliding mode-based trajectory tracking of LIMO mobile robots: Stability analysis and experimental validation

Saim Ahmed[1*], Zeeshan Haider[1], and Ahmad Taher Azar[1,2]

[1]Automated Systems and Computing Lab (ASCL), Prince Sultan University, Riyadh, Saudi Arabia
[2]College of Computer and Information Sciences, Prince Sultan University, Riyadh, Saudi Arabia
sahmed@psu.edu.sa, zhaider@psu.edu.sa, aazar@psu.edu.sa

ARTICLE INFO

Article history:
Received: July 10, 2026
Revised: August 11, 2026
Accepted: August 24, 2026
Published Online: September 2, 2026

Keywords:
Fixed-time sliding mode control
Trajectory tracking
Mobile robot
LIMO robot
Robust control

AMS Classification 2010:
26A33; 34A08; 35H15; 34K50; 47H10; 60H10

ABSTRACT

This paper proposes a two-layer robust fixed-time sliding mode control (FTSMC) scheme for the trajectory-tracking problem of a differential-drive LIMO mobile robot subject to modeling uncertainties and external disturbances. At the kinematic layer, a backstepping-based velocity command is designed to stabilize the posture error dynamics. At the dynamic layer, an integral-type nonsingular fixed-time sliding surface combined with a robust reaching law drives the velocity tracking errors to zero within a settling-time bound that is independent of the initial conditions. Unlike finite-time schemes, whose convergence time grows with the initial tracking error, the proposed method provides an explicit, pre-computable fixed-time guarantee while avoiding singularity and severe chattering. The main contribution is a rigorous fixed-time stability analysis with explicit settling-time bounds, together with a hardware-friendly control law that requires only the known upper bound of the lumped disturbance. Real-time experiments on the LIMO platform, conducted under both disturbance-free and disturbed conditions, confirm that the proposed FTSMC achieves the lowest Integral Squared Error (ISE), Integral Absolute Error (IAE), and Root Mean Square Error (RMSE) among the compared methods, reducing the ISE by up to a factor of 287, the IAE by up to a factor of 11, and the RMSE by up to a factor of 17. The findings demonstrate that the proposed scheme is a high-precision, hardware-friendly solution for real-time trajectory tracking of low-cost differential-drive mobile robots.

(cc) BY

1. Introduction

In recent decades, Wheeled Mobile Robots (WMRs) have gained significant attention due to their widespread applications in various domains, including industrial automation, agricultural monitoring, planetary exploration, and service robotics.[1,2] A fundamental requirement for the autonomous operation of these systems is the capability to track a predefined trajectory with high precision and robustness. However, high-performance trajectory tracking remains a challenging control problem due to the inherent nonholonomic kinematic constraints of WMRs, which restrict their instantaneous motion in the lateral direction. Furthermore, in practical scenarios, mobile robots are inevitably subject to complex uncertainties, such as parameter variations (e.g., mass and inertia changes), unmodeled dynamics, wheel slip/skid, and external disturbances, which can significantly degrade tracking accuracy and system stability.[3,4]

To address these challenges, various control strategies have been proposed in the literature, ranging from classical Proportional-Integral-Derivative (PID) control and backstepping techniques to more advanced nonlinear control methods. Among these, Sliding Mode Control (SMC)

*Corresponding Author

has emerged as a powerful robust control technique due to its invariance to matched uncertainties and its ability to reject external disturbances once the system states reach the sliding surface.[5] Despite its effectiveness, conventional linear SMC only guarantees asymptotic convergence of the tracking error to zero, implying that the convergence time may be infinite theoretically. Moreover, it often exhibits chattering—high-frequency oscillations in the control input—which can cause mechanical wear on actuators.[6–8]

To overcome the limitation of asymptotic convergence, Finite-Time Sliding Mode Control (FtSMC) and Terminal Sliding Mode Control (TSMC) strategies were developed, ensuring that system states converge to equilibrium in a finite time.[4,9] For instance, Moudoud *et al.*[4] proposed an extended state observer-based finite-time adaptive SMC to handle uncertainties and improve convergence speed. Similarly, Roy *et al.*[3] investigated time-delay SMC to handle nonholonomic constraints robustly. However, a critical drawback of finite-time control methods is that the convergence time function depends on the initial states of the system. As the initial error increases, the settling time grows, which may be undesirable for time-critical applications where a guaranteed convergence bound is required regardless of initial conditions.

This limitation led to the development of Fixed-Time Sliding Mode Control and Predefined-Time control strategies. In fixed-time stability theory, the upper bound of the settling time is independent of the initial states and can be pre-computed based on the controller parameters.[10,11] Extending this, Sun *et al.*[12] introduced a predefined-time TSMC that allows the convergence time to be set explicitly as a physical parameter in the controller. This property is particularly advantageous for mobile robots operating in dynamic environments where rapid and predictable response times are essential. Recent works have explored fixed-time control for WMRs; for example, Sun *et al.*[2] applied fixed-time SMC to mecanum-wheeled robots, and Moudoud *et al.*[1] developed an adaptive fixed-time scheme to handle unknown upper bounds of disturbances.

Despite these advancements, several weaknesses of the existing literature motivate this study. First, finite-time control methods cannot provide a convergence-time bound that is independent of the initial state, which limits their predictability in time-critical tasks. Second, many fixed-time sliding-mode schemes rely on complex adaptive mechanisms or high-order observers whose gains are difficult to tune on resource-constrained platforms. Third, most fixed-time WMR results are validated only through numerical simulations, and rigorous experimental validation on low-cost differential-drive platforms such as the LIMO robot remains scarce. Therefore, there remains a need for robust, fixed-time control strategies specifically tailored and validated for differential-drive platforms like the LIMO mobile robot, considering both kinematic and dynamic levels in the presence of realistic disturbances. This paper addresses this gap by proposing a Fixed-Time Sliding Mode Control strategy for the trajectory tracking of a real-time application of the LIMO mobile robot.

The novel features of the proposed work, relative to the existing literature, can be summarized as follows: (i) a two-layer kinematic-dynamic control architecture in which a backstepping-based velocity command is generated at the kinematic layer and tracked by an integral-type nonsingular fixed-time sliding surface at the dynamic layer, explicitly avoiding both the singularity problem of classical terminal sliding surfaces and the chattering of signum-based reaching laws; (ii) a rigorous fixed-time stability analysis providing explicit, pre-computable settling-time bounds that are independent of the initial tracking errors; and (iii) a hardware-friendly control law that requires only the known upper bound of the lumped disturbance, without adaptive mechanisms or observers, and is experimentally validated on the LIMO platform with quantitative performance indices.

The main contributions of this work are summarized as follows:

(1) Unlike most existing studies that treat the kinematic and dynamic layers separately, a complete two-layer kinematic-dynamic model of the differential-drive LIMO mobile robot is derived, and a backstepping-based kinematic controller is designed such that the posture error dynamics are stabilized while the dynamic layer concurrently enforces fixed-time convergence of the velocity errors.
(2) An integral-type nonsingular fixed-time sliding surface is designed. In contrast to conventional terminal sliding surfaces,[13,14] the proposed surface avoids the singularity problem and guarantees that the velocity tracking errors converge to the origin within an explicit settling-time bound that is independent of the initial tracking error.
(3) A robust fixed-time control law is developed whose discontinuous term uses only the known upper bound of the lumped disturbance. In contrast to adaptive or observer-b

ased schemes,[1,15] this avoids extra adaptation dynamics and reduces the implementation complexity, while a rigorous Lyapunov analysis proves fixed-time reachability of the sliding surface.

(4) The effective addition of this study is substantiated by a comprehensive experimental study on the LIMO platform under both disturbance-free and disturbed conditions, in which the proposed FTSMC achieves the lowest ISE, IAE, and RMSE among the compared methods, with quantitative reductions of up to 99.6% (ISE) and 90.2% (RMSE) relative to TDSMC, FOSTSMC, and AFtSMC, and generates notably smoother control inputs.

The remainder of this paper is organized as follows: Section 3 and 4 present the kinematic and dynamic modeling of the mobile robot. Section 5 details the error dynamics formulation. The design of the proposed fixed-time sliding mode controller and stability analysis are provided in Section 6. Experimental results and discussions are presented in Section 7, followed by the conclusion in Section 9.

2. Related work

The trajectory-tracking problem for Wheeled Mobile Robots (WMRs) has been a focal point of research in the control engineering community, driven by the increasing demand for autonomous systems in industrial logistics, service robotics, and hazardous-environment exploration.[2] A fundamental challenge in controlling WMRs lies in their nonholonomic kinematic constraints, which restrict instantaneous motion in the lateral direction, coupled with inevitable nonlinearities such as wheel slip, friction, and parameter uncertainties.[16] To address these issues, various advanced control strategies have been developed, with Sliding Mode Control (SMC) emerging as a dominant approach due to its inherent robustness against matched disturbances.

2.1. Evolution of sliding mode control strategies

Classical SMC, characterized by a linear sliding surface, has been extensively applied to WMRs to ensure asymptotic tracking stability. For instance, Roy *et al.*[3] investigated time-delay SMC to mitigate the effects of measurement delays in mobile robot navigation. However, the primary limitation of linear SMC is that the system states converge to the equilibrium point asymptotically, theoretically requiring infinite time. In time-critical applications where rapid response is essential, this asymptotic convergence is often insufficient.

To achieve finite-time convergence, Terminal Sliding Mode Control (TSMC) was introduced, employing nonlinear fractional-power terms in the sliding surface.[13] This concept has been further refined into Nonsingular Terminal SMC (NTSMC) to avoid the singularity problems inherent in standard TSMC. Recent works have demonstrated the efficacy of these methods; for example, Alnufaie[14] combined type-2 fuzzy logic with nonsingular fast terminal SMC to enhance robustness against unstructured uncertainties. Similarly, Sun *et al.*[17] proposed an adaptive super-twisting fast NTSMC for high-precision servo systems, a technique that is directly transferable to robotic platforms. As discussed above, the dependence of the settling time on the initial states remains the main drawback of these finite-time schemes.

2.2. Fixed-time stability and control

To overcome the dependence of the settling time on the initial conditions, the concept of fixed-time stability was established by Polyakov.[18] In fixed-time control, the settling time is bounded by a constant that is independent of the initial conditions, thereby providing a uniform guarantee on the convergence time. This property is particularly advantageous for wheeled mobile robots (WMRs) operating in dynamic environments where predictable convergence is important. Recent studies have demonstrated the effectiveness of fixed-time and predefined-time sliding-mode methodologies in a variety of nonlinear systems. For instance, Lai and Wang[19] developed finite- and fixed-time synchronization protocols for memristive chaotic systems using sliding-mode reaching laws, where the fixed-time design provides an upper bound on the convergence time independent of the initial conditions while reducing chattering and accelerating the reaching process. Lai *et al.*[20] further investigated diverse dynamical behaviors and predefined-time synchronization of a memristive chaotic system using a nonlinear sliding-mode framework, while Lai *et al.*[21] established fixed-time and predefined-time synchronization criteria for inertial memristive neural networks with proportional delay and mismatched switching jumps. These studies demonstrate the broad applicability of fixed-time and predefined-time sliding-mode methodologies and motivate their extension to trajectory-tracking problems in wheeled mobile robots.

Recent literature has seen a surge in applying fixed-time concepts to mobile robotics. Moudoud and Aissaoui[1] developed a fixed-time adaptive SMC for WMRs, validating its superiority over finite-time methods through real-time implementation. Ma *et al.*[10] proposed a fixed-time integral sliding mode scheme, utilizing a disturbance observer to enhance tracking accuracy. Furthermore, Sun *et al.*[2] introduced a novel fixed-time SMC for mecanum-wheeled robots, effectively handling the complex dynamics of omnidirectional motion. More recently, Nguyen *et al.*[16] integrated prescribed performance functions with fixed-time control to ensure that tracking errors remain within pre-defined bounds, providing both transient and steady-state performance guarantees.

2.3. Disturbance observation and robustness

In practical scenarios, WMRs are subject to complex disturbances including parameter variations, unmodeled dynamics, and external forces. To maintain high-precision tracking, robust control schemes often incorporate Disturbance Observers (DOBs) or Extended State Observers (ESOs), or neural-network-based adaptive control. Sun *et al.*[22] utilized adaptive neural tracking to manage manipulators under input saturation, ensuring robustness without requiring an exact dynamic model. In,[23] an adaptive dynamic programming approach was designed to solve a zero-sum game-based dynamic self-triggered SMC for continuous-time unknown nonlinear systems with asymmetric input constraints. Additionally, for systems requiring high efficiency, Chu and He[24] proposed a unified neural event-triggered approach that reduces computational burden by updating control laws only when necessary. Zhang *et al.*[15] demonstrated that integral sliding-mode observers can accurately estimate disturbances in Euler-Lagrangian systems. In the context of fixed-time control, Labbadi *et al.*[25] addressed the challenge of mismatched disturbances, proposing a robust fixed-time strategy that ensures global stability. Fang *et al.*[26] further extended this by combining disturbance observers with fault-tolerant control, ensuring system reliability even under actuator faults. These works highlight the necessity of active disturbance compensation in modern robust control design.

2.4. Formation control of differential-drive mobile robots

Beyond single-robot trajectory tracking, cooperative multi-robot systems have recently attracted considerable attention, and several instructive works are directly relevant to the control of differential-drive mobile robots. Karam *et al.*[27] proposed a unified kinematic-dynamic intelligent formation control scheme that combines a geometric integral sliding mode controller with type-2 adaptive fuzzy PID controllers for differential-drive mobile robots, achieving robust formation tracking under model uncertainties. In addition, Karam *et al.*[28] developed a formation control strategy based on an adaptive-τ Tustin differentiator for real-time estimation of the leader's velocity, which avoids the need for direct velocity measurements from the leader. These works highlight that the combination of kinematic-dynamic control architectures with robust sliding-mode techniques constitutes an effective design paradigm for mobile robots, further motivating the two-layer kinematic-dynamic fixed-time framework adopted in this study.

2.5. Gaps in existing literature

Despite the significant progress in fixed-time control for WMRs, several gaps remain in the existing literature. First, many proposed fixed-time schemes suffer from algebraic complexity and potential singularity issues, requiring complex switching mechanisms that can induce chattering. Second, the convergence-time bounds of most finite-time schemes depend on the initial state, which severely limits their predictability in time-critical applications. Third, while theoretical developments are abundant, rigorous experimental validation on low-cost, resource-constrained platforms like the LIMO robot remains limited, as many studies rely solely on numerical simulations or high-end laboratory setups. Fourth, the simultaneous handling of fast time-varying disturbances and large initial errors without compromising the fixed-time convergence guarantee is still an open challenge, since most existing adaptive laws for SMC do not fully guarantee fixed-time convergence of the adaptation parameters themselves. These weaknesses are precisely what motivates the present work.

2.6. Motivation and contribution

Motivated by these challenges, this paper proposes a robust Fixed-Time Sliding Mode Control (FTSMC) strategy specifically tailored for the LIMO mobile robot. Unlike standard finite-time approaches, the proposed method guarantees convergence within a user-defined time bound regardless of the initial tracking error. By integrating a nonsingular fixed-time sliding surface with a robust control law, this work aims to eliminate the

singularity problem while ensuring high-precision tracking. The theoretical contributions are substantiated by comprehensive experimental validation on the LIMO platform, demonstrating the practical applicability and robustness of the proposed strategy in real-world conditions.

3. Kinematic modeling of mobile robot

The LIMO mobile robot is a differential-drive platform moving on a planar surface. Its configuration is described by the vector $q = [x, y, \theta]^T$, where (x, y) denotes the position of the robot's center of mass (COM) in the global inertial frame, and θ represents the heading angle of the robot. The kinematic equations of motion can be expressed as:

$$\dot{q} = J(q)\eta \tag{1}$$

where $\eta = [\upsilon, \omega]^T$ is the vector of linear and angular velocities of the robot, and $J(q)$ is the transformation matrix defined as:

$$J(q) = \begin{bmatrix} \cos\theta & 0 \\ \sin\theta & 0 \\ 0 & 1 \end{bmatrix} \tag{2}$$

Under the assumption of pure rolling and no slipping, the robot satisfies the nonholonomic constraint $\dot{y}\cos\theta - \dot{x}\sin\theta = 0$, which prevents instantaneous lateral motion.

4. Dynamic modeling

The dynamic model of the differential-drive mobile robot can be derived using the Euler-Lagrange formulation. The dynamic equations, including the nonholonomic constraints, are given by:[29]

$$M(q)\ddot{q} + C(q,\dot{q})\dot{q} + G(q) = B(q)\tau + \tau_{dist} - A^T(q)\lambda \tag{3}$$

where $M(q) \in \mathbb{R}^{3\times3}$ is the symmetric positive-definite inertia matrix, $C(q,\dot{q}) \in \mathbb{R}^{3\times3}$ represents the centripetal and Coriolis forces, $G(q) \in \mathbb{R}^3$ denotes the gravitational vector, $B(q) \in \mathbb{R}^{3\times2}$ is the input transformation matrix, $\tau = [\tau_R, \tau_L]^T$ is the control input vector consisting of the torques applied to the right and left wheels, τ_{dist} is a bounded disturbance vector (i.e., the disturbance is unknown but bounded, as is the case for the external loads and unmodeled friction considered in this work), $A(q)$ is the constraint matrix, and λ is the vector of Lagrange multipliers representing the constraint forces.

The system matrices are defined as

$$M(q) = \begin{bmatrix} m & 0 & 0 \\ 0 & m & 0 \\ 0 & 0 & I \end{bmatrix}, \quad C(q,\dot{q}) = \begin{bmatrix} 0 & 0 & -m\dot{y} \\ 0 & 0 & m\dot{x} \\ -m\dot{y} & m\dot{x} & 0 \end{bmatrix} \tag{4}$$

$$B(q) = \frac{1}{r}\begin{bmatrix} \cos\theta & \cos\theta \\ \sin\theta & \sin\theta \\ L & -L \end{bmatrix}, \quad A^T(q) = \begin{bmatrix} -\sin\theta \\ \cos\theta \\ 0 \end{bmatrix}$$
$$\lambda = -m(\dot{x}_c\cos\theta + \dot{y}_c\sin\theta)\dot{\theta}$$

where m is the mass of the robot, I is the moment of inertia about the vertical axis, r is the radius of the wheels, and L is the half-width of the robot base. Since the robot moves on a horizontal plane, the gravitational term $G(q)$ is zero.

To facilitate controller design, it is convenient to express the dynamics in terms of the body velocities η. Differentiating **Equation (1)** with respect to time yields $\ddot{q} = \dot{J}(q)\eta + J(q)\dot{\eta}$. Substituting this into **Equation (3)** and multiplying by $J^T(q)$ to eliminate the constraint forces (since $J^T A^T = 0$), we obtain the reduced dynamic model:

$$\bar{M}\dot{\eta} + \bar{C}\eta = \bar{B}\tau + J^T\tau_{dist} \tag{5}$$

where $\bar{M} = J^T M J$, $\bar{C} = J^T(M\dot{J} + CJ)$, and $\bar{B} = J^T B$. Evaluating these matrices yields:

$$\bar{M} = \begin{bmatrix} m & 0 \\ 0 & I \end{bmatrix}, \quad \bar{B} = \begin{bmatrix} \frac{1}{r} & \frac{1}{r} \\ \frac{L}{r} & -\frac{L}{r} \end{bmatrix} \tag{6}$$

Note that the term $\bar{C}$ vanishes because the center of mass is assumed to coincide with the geometric center. The simplified dynamic equation governing the velocity evolution is then:

$$\dot{\eta} = \bar{M}^{-1}\bar{B}\tau + \bar{M}^{-1}J^T\tau_{dist} = \Pi\tau + \tau_d \tag{7}$$

where $\tau_d = \bar{M}^{-1}J^T\tau_{dist}$ is the lumped disturbance expressed in the robot body frame and Π is the inverse inertial matrix scaled by the wheel geometry:

$$\Pi = \begin{bmatrix} \frac{1}{mr} & \frac{1}{mr} \\ \frac{L}{Ir} & -\frac{L}{Ir} \end{bmatrix} \tag{8}$$

Since the disturbance torque τ_{dist} is bounded, i.e., $\|\tau_{dist}\| \le \bar{\tau}_{dist}$ with $\bar{\tau}_{dist} > 0$, and the matrices $\bar{M}^{-1}$ and J have bounded norms, the lumped disturbance τ_d is also bounded and satisfies

$$|\tau_{d,i}| \le \mathcal{D}, \quad i = 1, 2, \tag{9}$$

where $\mathcal{D} = \|\bar{M}^{-1}J^T\|\,\bar{\tau}_{dist} > 0$ is the known disturbance upper bound. This bound is the only information about the disturbance required by the control law in Section 6, where the discontinuous term $\mathcal{D}\,\mathrm{sign}(s)$ compensates the disturbance component-wise. **Equation (7)** relates the control torques directly to the acceleration of the mobile robot, serving as the basis for the proposed dynamic control design.

5. Posture error and kinematic control

The objective of the trajectory tracking problem

is to make the actual robot pose $q = [x, y, \theta]^T$ converge to a time-varying reference trajectory $q_r = [x_r, y_r, \theta_r]^T$. The reference trajectory is generated by a virtual reference robot satisfying:

$$\dot{q}_r = \begin{bmatrix} \upsilon_r \cos\theta_r \\ \upsilon_r \sin\theta_r \\ \omega_r \end{bmatrix} \tag{10}$$

where υ_r and ω_r are the reference linear and angular velocities. The tracking error vector $e = [e_1, e_2, e_3]^T$ is defined in the robot's local frame as:

$$\begin{bmatrix} e_1 \\ e_2 \\ e_3 \end{bmatrix} = \begin{bmatrix} \cos\theta & \sin\theta & 0 \\ -\sin\theta & \cos\theta & 0 \\ 0 & 0 & 1 \end{bmatrix} \begin{bmatrix} x_r - x \\ y_r - y \\ \theta_r - \theta \end{bmatrix} \tag{11}$$

Taking the time derivative of **Equation (11)** yields the kinematic error dynamics:

$$\begin{bmatrix} \dot{e}_1 \\ \dot{e}_2 \\ \dot{e}_3 \end{bmatrix} = \begin{bmatrix} \omega e_2 + \upsilon_r \cos e_3 - \upsilon \\ -\omega e_1 + \upsilon_r \sin e_3 \\ \omega_r - \omega \end{bmatrix} \tag{12}$$

To stabilize the kinematic error dynamics, a virtual kinematic control law (velocity command) $\eta_c = [\upsilon_c, \omega_c]^T$ is designed using the backstepping technique:

$$\begin{bmatrix} \upsilon_c \\ \omega_c \end{bmatrix} = \begin{bmatrix} \upsilon_r \cos e_3 + \kappa_1 e_1 \\ \omega_r + \kappa_2 \upsilon_r e_2 + \kappa_3 \sin e_3 \end{bmatrix} \tag{13}$$

where $\kappa_1, \kappa_2, \kappa_3 > 0$ are positive control gains.

Remark 1: The stability of this kinematic controller can be verified using the Lyapunov candidate function:

$$V_1 = \frac{1}{2}(e_1^2 + e_2^2) + \frac{1 - \cos e_3}{\kappa_2} \tag{14}$$

The time derivative of V_1 is:

$$\begin{aligned} &\dot{V}_1 = e_1\dot{e}_1 + e_2\dot{e}_2 + \tfrac{\sin(e_3)}{\kappa_2}\dot{e}_3 \\ &\dot{V}_1 = e_1(\omega e_2 + \upsilon_r \cos e_3 - \upsilon) \\ &+e_2(-\omega e_1 + \upsilon_r \sin e_3) \\ &+\tfrac{\sin(e_3)}{\kappa_2}(\omega_r - \omega) \end{aligned} \tag{15}$$

$$\dot{V}_1 = -\kappa_1 e_1^2 - \frac{\kappa_3}{\kappa_2}\sin^2 e_3 \leq 0 \tag{16}$$

This implies that if the actual velocities η perfectly track the command velocities η_c, the posture error e converges to zero asymptotically. The task of the subsequent dynamic controller is to ensure that $\eta \to \eta_c$ in finite or fixed time.

6. Fixed-time sliding mode control design

In this section, a Fixed-Time Sliding Mode Controller (FTSMC) is developed to track the desired velocities generated by the kinematic controller. The primary objective is to drive the velocity tracking errors to zero within a fixed time bounded by a constant, regardless of the initial conditions.

6.1. Velocity error dynamics

Define the velocity tracking error vector $\bar{e} = [\bar{e}_1, \bar{e}_2]^T$ as the difference between the command velocities η_c and the actual robot velocities η:

$$\bar{e} = \eta_c - \eta = \begin{bmatrix} \upsilon_c - \upsilon \\ \omega_c - \omega \end{bmatrix} \tag{17}$$

Differentiating **Equation (17)** with respect to time and substituting the robot dynamics from **Equation (7)**, the open-loop error dynamics are obtained as:

$$\dot{\bar{e}} = \dot{\eta}_c - \dot{\eta} = \dot{\eta}_c - \Pi\tau - \tau_d \tag{18}$$

6.2. Fixed-time sliding surface design

To guarantee fixed-time convergence of the tracking error, an integral-type nonsingular sliding surface $s \in \mathbb{R}^2$ is defined as follows:

$$s = \bar{e} + \int \left(k_1 \mathrm{sig}(\bar{e})^\alpha + k_2 \mathrm{sig}(\bar{e})^\beta\right) dt \tag{19}$$

where $\mathrm{sig}(\cdot)^\gamma = |\cdot|^\gamma \mathrm{sign}(\cdot)$ denotes the element-wise signed power function. The parameters are chosen such that $k_1, k_2 > 0$ are positive diagonal gain matrices, $0 < \alpha < 1$, and $\beta > 1$.

Lemma 1. [30] *Let V be a positive-definite function. If $\dot{V} \leq -aV^p - bV^q$ with $a, b > 0$, $0 < p < 1$, and $q > 1$, then the origin is fixed-time stable and the settling time is bounded by*

$$T \leq \frac{1}{a(1-p)} + \frac{1}{b(q-1)}. \tag{20}$$

Lemma 2. [31] *In addition, for $x_i \in \mathbb{R}$, $i = 1, \ldots, n$, the following inequalities hold: $\left(\sum_{i=1}^n x_i^2\right)^p \leq \sum_{i=1}^n |x_i|^{2p}$ for $0 < p \leq 1$, and $\left(\sum_{i=1}^n x_i^2\right)^q \leq n^{q-1}\sum_{i=1}^n |x_i|^{2q}$ for $q \geq 1$.*

The convergence of the velocity tracking error is analyzed using $V_2 = \frac{1}{2}\bar{e}^T\bar{e}$. Under the sliding manifold condition ($\dot{s} = 0$), the error derivative follows the fixed-time law. Substituting this into $\dot{V}_2$ yields

$$\dot{V}_2 = \bar{e}^T\dot{\bar{e}} \tag{21}$$

when $\dot{s} = 0$, $\dot{\bar{e}} = -k_1\mathrm{sig}(\bar{e})^\alpha - k_2\mathrm{sig}(\bar{e})^\beta$, we have

$$\dot{V}_2 = \bar{e}^T\left(-k_1\mathrm{sig}(\bar{e})^\alpha - k_2\mathrm{sig}(\bar{e})^\beta\right) \tag{22}$$

$$\begin{aligned} \dot{V}_2 &= -\sum_{i=1}^{2} k_{1i}|\bar{e}_i|^{\alpha+1} - \sum_{i=1}^{2} k_{2i}|\bar{e}_i|^{\beta+1} \\ &= -\sum_{i=1}^{2} k_{1i}\left(|\bar{e}_i|^2\right)^{\frac{\alpha+1}{2}} - \sum_{i=1}^{2} k_{2i}\left(|\bar{e}_i|^2\right)^{\frac{\beta+1}{2}} \end{aligned} \tag{23}$$

Then, according to Lemma 2, this can be written as

$$\begin{aligned}\dot{V}_2 \leq & -\min(k_{1i})\left(\sum_{i=1}^{2}\bar{e}_i^2\right)^{\frac{\alpha+1}{2}} \\ & -\min(k_{2i})2^{\frac{1-\beta}{2}}\left(\sum_{i=1}^{2}\bar{e}_i^2\right)^{\frac{\beta+1}{2}}\end{aligned} \tag{24}$$

$$\begin{aligned}\dot{V}_2 \leq & -\min(k_{1i})(2V_2)^{\frac{\alpha+1}{2}} \\ & -\min(k_{2i})2^{\frac{1-\beta}{2}}(2V_2)^{\frac{\beta+1}{2}}\end{aligned} \tag{25}$$

According to fixed-time stability theory Lemma 1, the equilibrium $\bar{e}$ is fixed-time stable. The settling time T_s is bounded by:

$$\begin{aligned}T_s \leq & \frac{2}{\min(k_{1i})2^{\frac{\alpha+1}{2}}(1-\alpha)} \\ & +\frac{1}{\min(k_{2i})(\beta-1)}\end{aligned} \tag{26}$$

where $\min(k_{1i})$ and $\min(k_{2i})$ denote the minimum diagonal entries of the gain matrices k_1 and k_2, respectively. This implies that the velocity tracking errors will converge to zero within a fixed time T_s after the sliding phase is established, irrespective of the initial condition.

6.3. Controller derivation and stability analysis

The control objective is to force the system state to reach the sliding surface $s = 0$ in fixed time and maintain it there. The time derivative of the sliding surface is given by:

$$\begin{aligned}\dot{s} &= \dot{\bar{e}} + k_1\mathrm{sig}(\bar{e})^{\alpha} + k_2\mathrm{sig}(\bar{e})^{\beta} \\ &= \dot{\eta}_c - \Pi\tau - \tau_d + k_1\mathrm{sig}(\bar{e})^{\alpha} + k_2\mathrm{sig}(\bar{e})^{\beta}\end{aligned} \tag{27}$$

To ensure the fixed-time reachability of the sliding surface, the control law is designed as:

$$\begin{aligned}\tau = \Pi^{-1}\Big(&\dot{\eta}_c - \mathcal{D}\,\mathrm{sign}(s) + k_1\,\mathrm{sig}(\bar{e})^{\alpha} \\ &+ k_2\,\mathrm{sig}(\bar{e})^{\beta} \\ &+ K_1\,\mathrm{sig}(s)^{\bar{\alpha}} + K_2\,\mathrm{sig}(s)^{\bar{\beta}}\Big)\end{aligned} \tag{28}$$

where $K_1, K_2 > 0$ are positive definite diagonal gain matrices, $0 < \bar{\alpha} < 1$, and $\bar{\beta} > 1$. The discontinuous term $\mathcal{D}\,\mathrm{sign}(s)$ is designed to dominate the bounded lumped disturbance τ_d componentwise ($|\tau_{d,i}| \leq \mathcal{D}$ in Section 4), so that no observer or adaptive mechanism is required. The overall architecture of the proposed scheme, consisting of a kinematic layer (posture-error backstepping control) and a dynamic layer (fixed-time sliding-mode velocity control), is depicted in **Figure 1**.

Theorem 1. *Consider the dynamic model of the LIMO mobile robot given by **Equation (7)** and the sliding surface defined in **Equation (19)**. Under the control law* (28)*, the closed-loop system is fixed-time stable, and the tracking errors converge to zero within a bounded time.*

Proof. Consider the Lyapunov candidate function:

$$V_3 = \frac{1}{2}s^T s \tag{29}$$

Taking the time derivative of V_3 yields:

$$\dot{V}_3 = s^T\dot{s} \tag{30}$$

Substituting **Equation (27)** and the control law (28) into $\dot{V}_3$ yields:

$$\dot{V}_3 = s^T\begin{pmatrix}\dot{\eta}_c - \begin{pmatrix}\dot{\eta}_c - \mathcal{D}sign(s) \\ +k_1\mathrm{sig}(\bar{e})^{\alpha}+k_2\mathrm{sig}(\bar{e})^{\beta} \\ +K_1\mathrm{sig}(s)^{\bar{\alpha}} + K_2\mathrm{sig}(s)^{\bar{\beta}}\end{pmatrix} \\ -\tau_d + k_1\mathrm{sig}(\bar{e})^{\alpha} + k_2\mathrm{sig}(\bar{e})^{\beta}\end{pmatrix} \tag{31}$$

By solving the above equation and using the bounded disturbance condition, we get

$$\begin{aligned}\dot{V}_3 &\leq s^T\left(-K_1\mathrm{sig}(s)^{\bar{\alpha}} - K_2\mathrm{sig}(s)^{\bar{\beta}}\right) \\ &\leq -\min(K_{1i})\sum_{i=1}^{2}|s_i|^{\bar{\alpha}+1} \\ &\quad -\min(K_{2i})\sum_{i=1}^{2}|s_i|^{\bar{\beta}+1} \\ &\leq -\min(K_{1i})\sum_{i=1}^{2}\left(|s_i|^2\right)^{\frac{\bar{\alpha}+1}{2}} \\ &\quad -\min(K_{2i})\sum_{i=1}^{2}\left(|s_i|^2\right)^{\frac{\bar{\beta}+1}{2}}\end{aligned} \tag{32}$$

Then, according to Lemma 2, this equation can be expressed as

$$\begin{aligned}\dot{V}_3 \leq & -\min(K_{1i})\left(\sum_{i=1}^{2}|s|_i^2\right)^{\frac{\bar{\alpha}+1}{2}} \\ & -\min(K_{2i})2^{\frac{1-\bar{\beta}}{2}}\left(\sum_{i=1}^{2}|s|_i^2\right)^{\frac{\bar{\beta}+1}{2}}\end{aligned} \tag{33}$$

$$\begin{aligned}\dot{V}_3 \leq & -\min(K_{1i})(2V_3)^{\frac{\bar{\alpha}+1}{2}} \\ & -\min(K_{2i})2^{\frac{1-\bar{\beta}}{2}}(2V_3)^{\frac{\bar{\beta}+1}{2}}\end{aligned} \tag{34}$$

This inequality satisfies the condition for fixed-time stability using Lemma 1. Consequently, the sliding surface $s = 0$ is reached within a fixed time T_r, bounded by:

$$\begin{aligned}T_r \leq & \frac{2}{\min(K_{1i})2^{\frac{\bar{\alpha}+1}{2}}(1-\bar{\alpha})} \\ & +\frac{1}{\min(K_{2i})(\bar{\beta}-1)}\end{aligned} \tag{35}$$

Once $s = 0$ is reached, the error dynamics evolve according to **Equation (19)**, ensuring fixed-time convergence of the velocity tracking error $\bar{e}$ to zero. This completes the proof. □

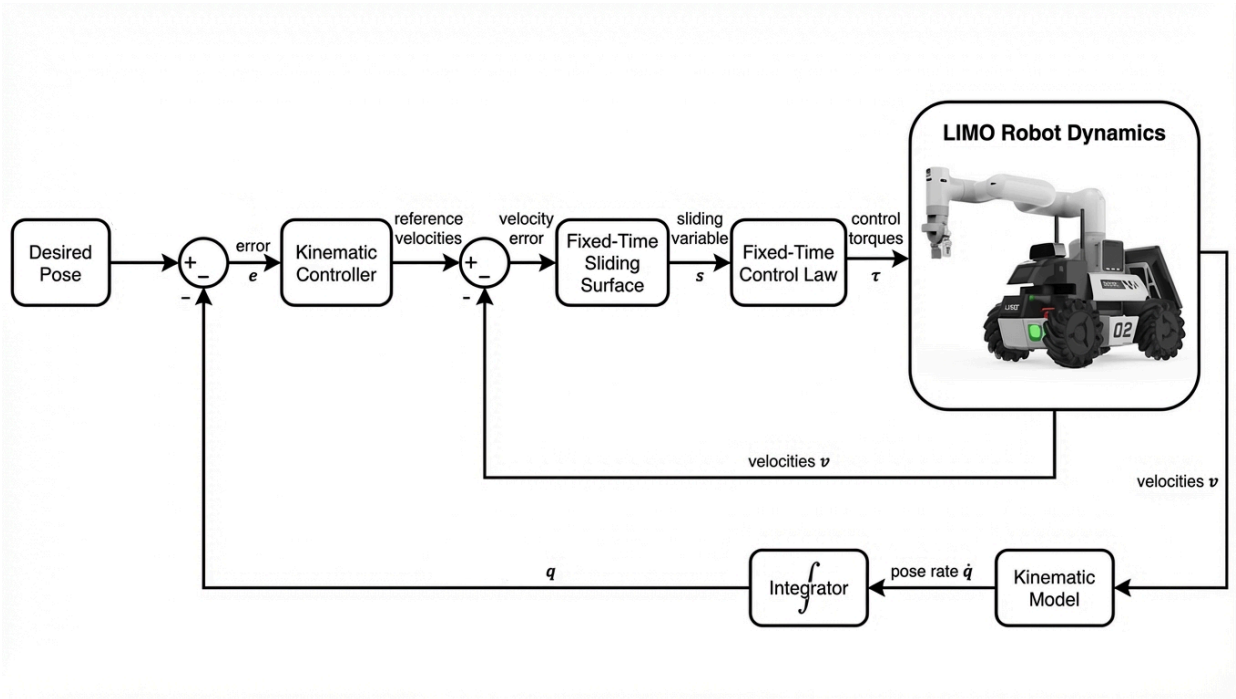


Figure 1. General block diagram of the proposed fixed-time sliding mode control scheme

The step-by-step implementation of the proposed scheme is summarized as pseudo-code in Algorithm 1.

Algorithm 1 Pseudo-code of the proposed FTSMC scheme.

Require: Robot parameters m, I, r, L; reference trajectory $q_r(t)$ with υ_r, ω_r; control gains κ_1, κ_2, κ_3, k_1, k_2, K_1, K_2; exponents α, β, $\bar{\alpha}$, $\bar{\beta}$; disturbance bound $\mathcal{D}$.

Ensure: Wheel torques $\tau = [\tau_R, \tau_L]^T$.

repeat

Measure the robot pose $q = [x, y, \theta]^T$ and velocities $\eta = [\upsilon, \omega]^T$ from the wheel encoders and IMU.

Compute the posture tracking error e using **Equation (11)**.

Compute the reference velocity commands $\eta_c = [\upsilon_c, \omega_c]^T$ using the kinematic backstepping law in **Equation (13)**.

Compute the velocity tracking error $\bar{e} = \eta_c - \eta$.

Compute the integral-type sliding surface s using **Equation (19)**.

Compute the control torques τ using the control law in **Equation (28)**.

Apply τ to the wheel actuators and proceed to the next sampling instant.

until Tracking task is completed

7. Experimental results and discussion

To validate the effectiveness and superiority of the proposed Fixed-Time Sliding Mode Control (FTSMC) strategy, real-time experiments were conducted on the LIMO mobile robot platform. The proposed method was compared with three existing control techniques: Time-Delay Sliding Mode Control (TDSMC),[3] Fractional-order Super-Twisting Sliding Mode Control (FOSTSMC),[29] and Adaptive Finite-time Sliding Mode Control (AFtSMC).[32]

7.1. Experimental setup

The experiments were performed on the LIMO multi-modal mobile robot, a differential-drive platform equipped with high-resolution quadrature encoders mounted on the two driving wheels and a nine-axis inertial measurement unit (IMU). The robot pose used for feedback was obtained by fusing wheel odometry with IMU measurements within the ROS navigation framework, which provides the position and heading estimates required by the kinematic layer of the proposed scheme. The control algorithms were implemented on the robot's onboard computer (NVIDIA Jetson Nano) under the Robot Operating System (ROS), and the control loop was executed at a sampling time of $T = 0.01$ s. A circle with a radius of 0.2 m was selected as the reference trajectory. The proposed control parameters, selected in accordance with the stability constraints of the proposed design (i.e., $k_1, k_2 > 0$, $0 < \alpha < 1$, $\beta > 1$, $K_1, K_2 > 0$, $0 < \bar{\alpha} < 1$, $\bar{\beta} > 1$), are $\kappa_1 = 8\,, \kappa_2 = 30\,, \kappa_3 = 22$, $k_1 = 0.001\,, k_2 = 0.001$, $K_1 = 1.5\,, K_2 = 1.3$, $\alpha =$

$0.7\,, \beta = 1.3\,, \alpha = 0.8\,, \bar{\beta} = 1.2$.

The tracking performance was evaluated using a circular reference trajectory of radius 0.2 m, which continuously exercises the robot's ability to handle a constant curvature while rejecting disturbances. The initial posture of the robot was set to coincide with the reference trajectory to evaluate the tracking maintenance performance. The experimental platform is shown in **Figure 2**.

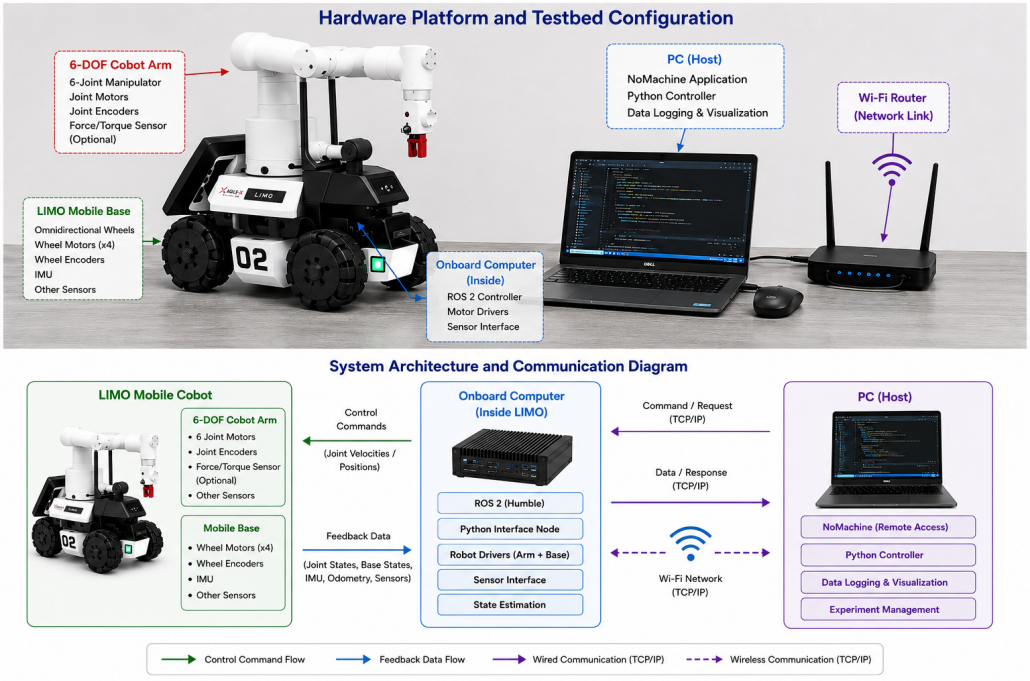


Figure 2. Experimental setup of the LIMO mobile robot platform

7.2. Case-1: without disturbance

7.2.1. Trajectory tracking performance

The trajectory tracking results of the LIMO robot compared with the three control schemes are depicted in **Figure 3**. all three controllers are capable of tracking the reference path. However, the proposed FTSMC strategy demonstrates superior tracking accuracy, with the actual robot trajectory (red solid line) coinciding almost perfectly with the reference path (black dashed line). In contrast, TDSMC (blue dash-dotted line), FOSTSMC (green dotted line), and AFtSMC (purple dash-dotted) exhibit visible deviations, particularly during curved sections where the dynamic effects are more pronounced.

7.2.2. Tracking error analysis

To provide a more detailed analysis of tracking precision, the time evolution of the position tracking errors in the X and Y directions is presented in **Figures 4** and **5**, respectively.

Figure 4 shows the tracking error along the X-axis. The proposed FTSMC achieves the fastest convergence and maintains the error within a significantly smaller bound than the other methods. The fixed-time stability property ensures that the error converges to a neighborhood of the origin independent of the initial conditions, providing robust performance. FOSTSMC performs better than TDSMC but still exhibits larger oscillations and steady-state error than the proposed method.

To provide a rigorous quantitative evaluation of the tracking performance, a steady-state error bound of ± 0.01 m was established as the convergence criterion. This threshold was selected based on the physical dimensions and odometry precision of the LIMO platform. As illustrated by the shaded regions in the error plots, the proposed FTSMC algorithm successfully drives the lateral and longitudinal errors into this bound within a deterministic timeframe. The inclusion of these bounds visually confirms the "practical stability" of the system, ensuring that the robot maintains high precision without inducing the mechanical chatter that typically degrades real-time feasibility in robotic-arm-equipped platforms.

Similarly, **Figure 5** illustrates the tracking error along the Y-axis. TDSMC suffers from significant deviations, reaching errors up to 0.014 m. FOSTSMC reduces this error but still shows fluctuations.

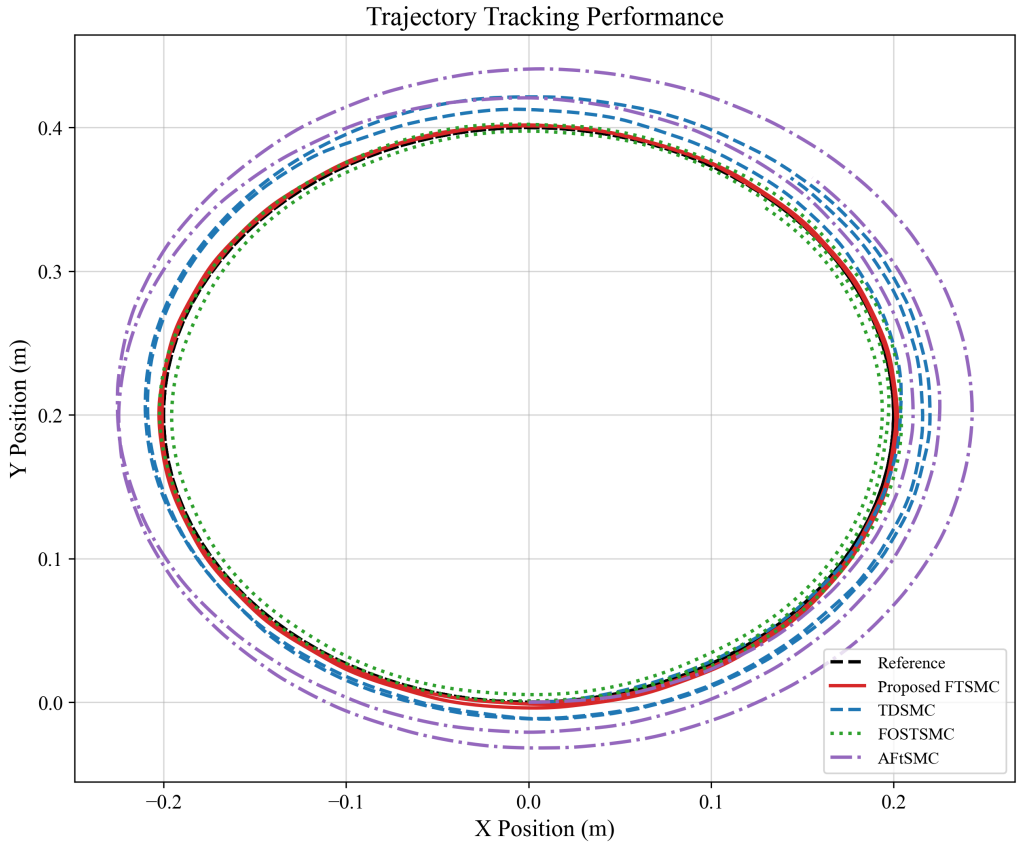


Figure 3. Comparison of trajectory tracking performance in the X-Y plane

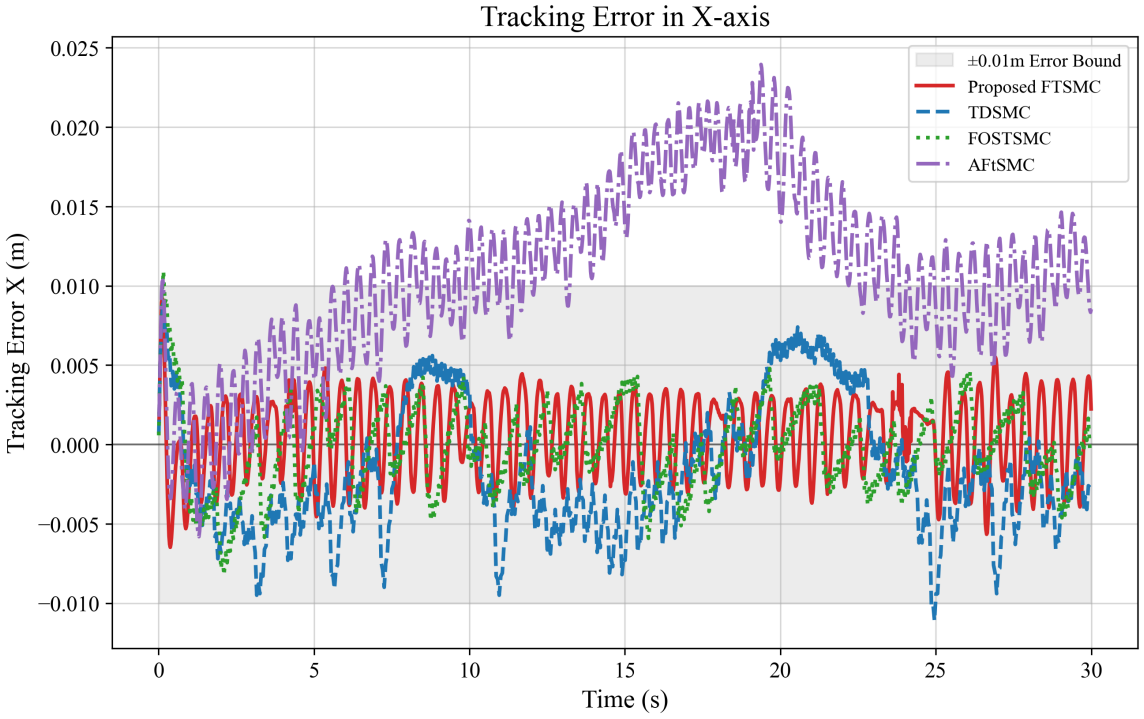


Figure 4. Time evolution of tracking error in X-axis

7.2.3. Velocity tracking analysis

To display the velocity variables of the mobile robot, the time evolution of the commanded and actual linear and angular velocities under the proposed FTSMC are presented in **Figures 6** and **7**.

The actual velocities v and ω track their commanded values v_c and ω_c closely and smoothly, confirming that the dynamic layer of the proposed scheme enforces velocity tracking with high fidelity while avoiding the chattering typical of signum-based sliding-mode controllers.

7.2.4. Control input analysis

The smooth generation of control inputs is crucial for actuator longevity and energy efficiency. **Figures 8** and **9** display the left wheel torque (τ_L) and right wheel torque (τ_R) control inputs.

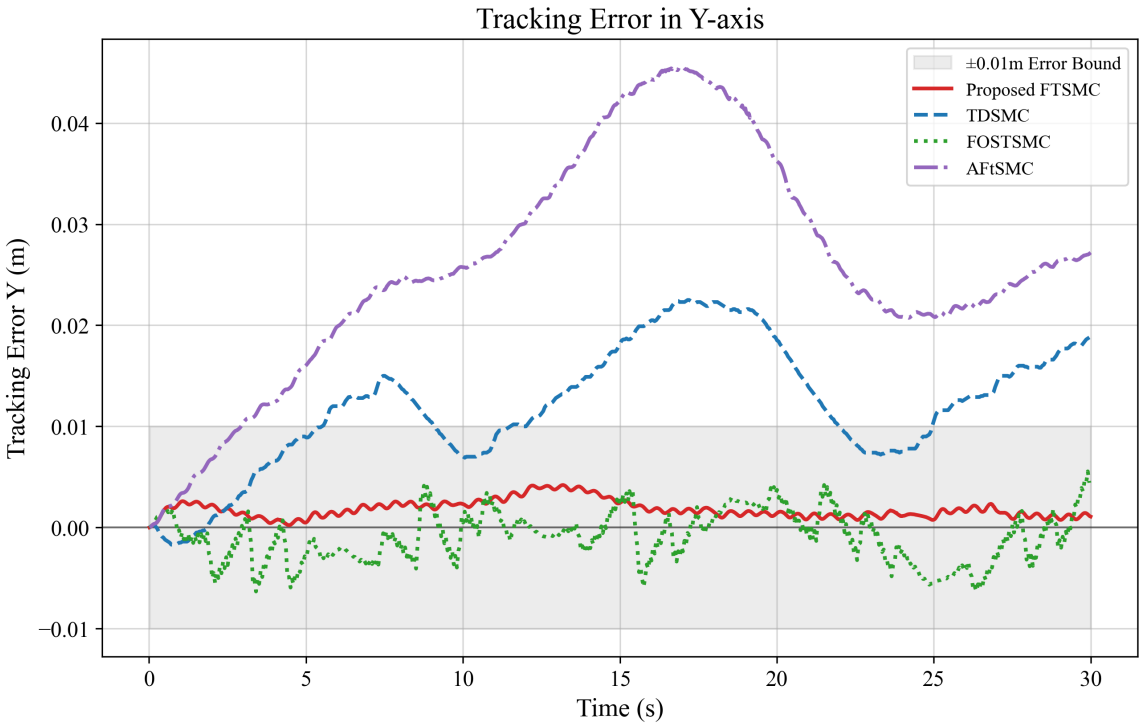


Figure 5. Time evolution of tracking error in Y-axis

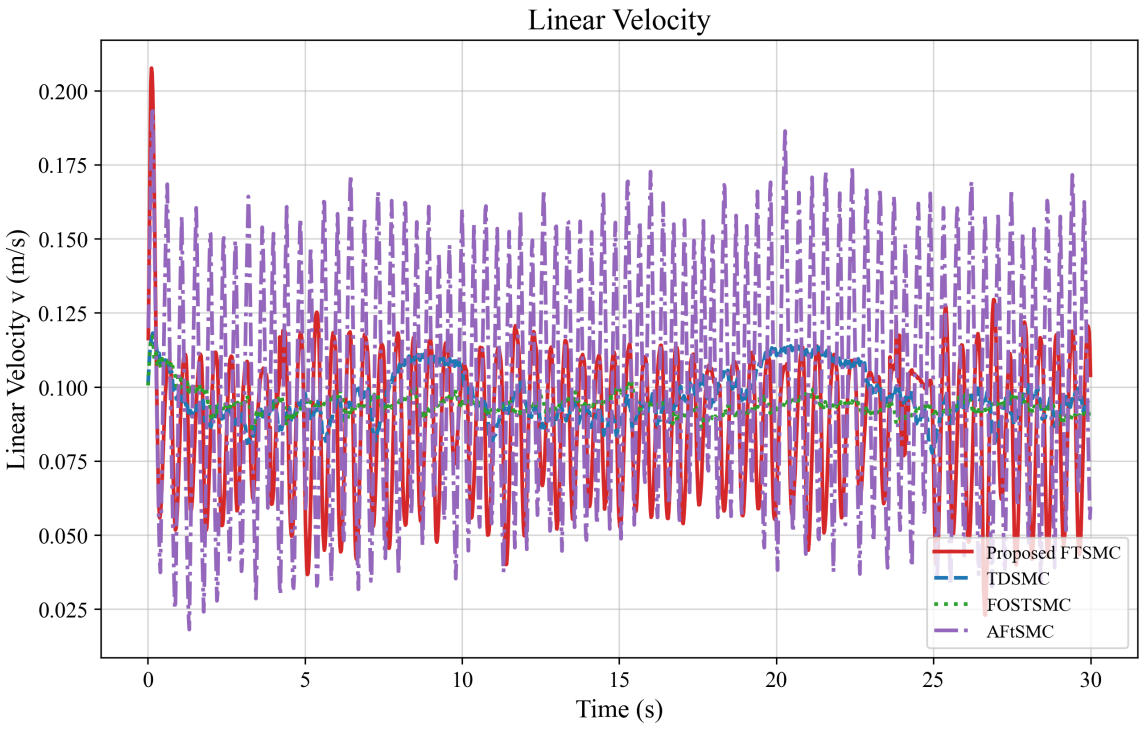


Figure 6. Linear velocity tracking (v_c vs. v) without disturbance

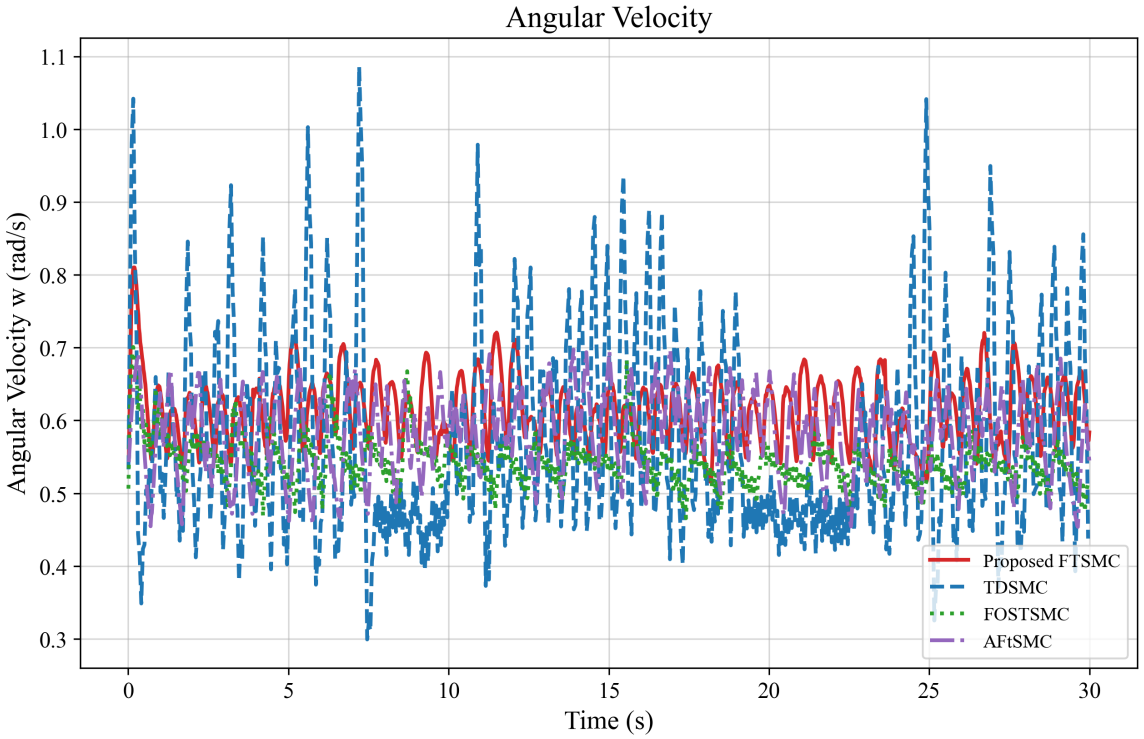


Figure 7. Angular velocity tracking (ω_c vs. ω) without disturbance

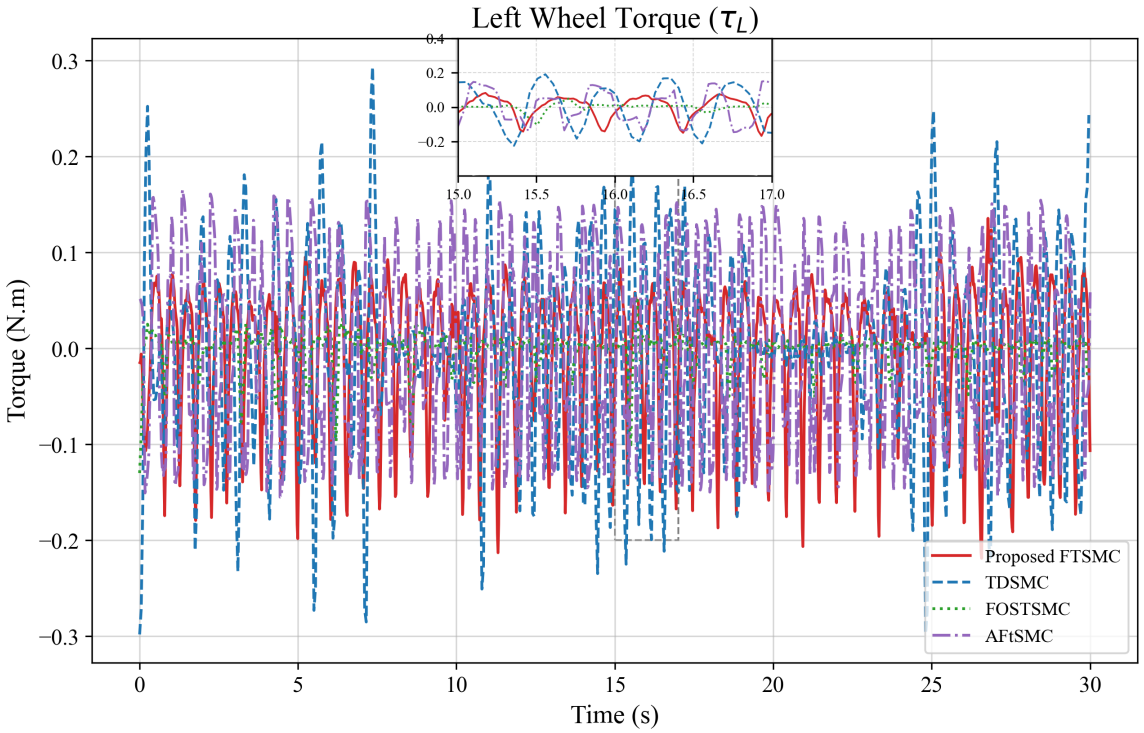


Figure 8. Control input: τ_L without disturbance

7.3. Case-2: with disturbance

In this subsection, the experiment was conducted under applied disturbances: $\tau_{dv}(t) = 0.15\sin(2t) + \begin{cases} 0.7 & 7.0 < t < 7.5 \\ 0 & \text{otherwise} \end{cases}$ and $\tau_{dw}(t) = 0.10\cos(2t) + \begin{cases} 0.7 & 7.0 < t < 7.5 \\ 0 & \text{otherwise} \end{cases}$

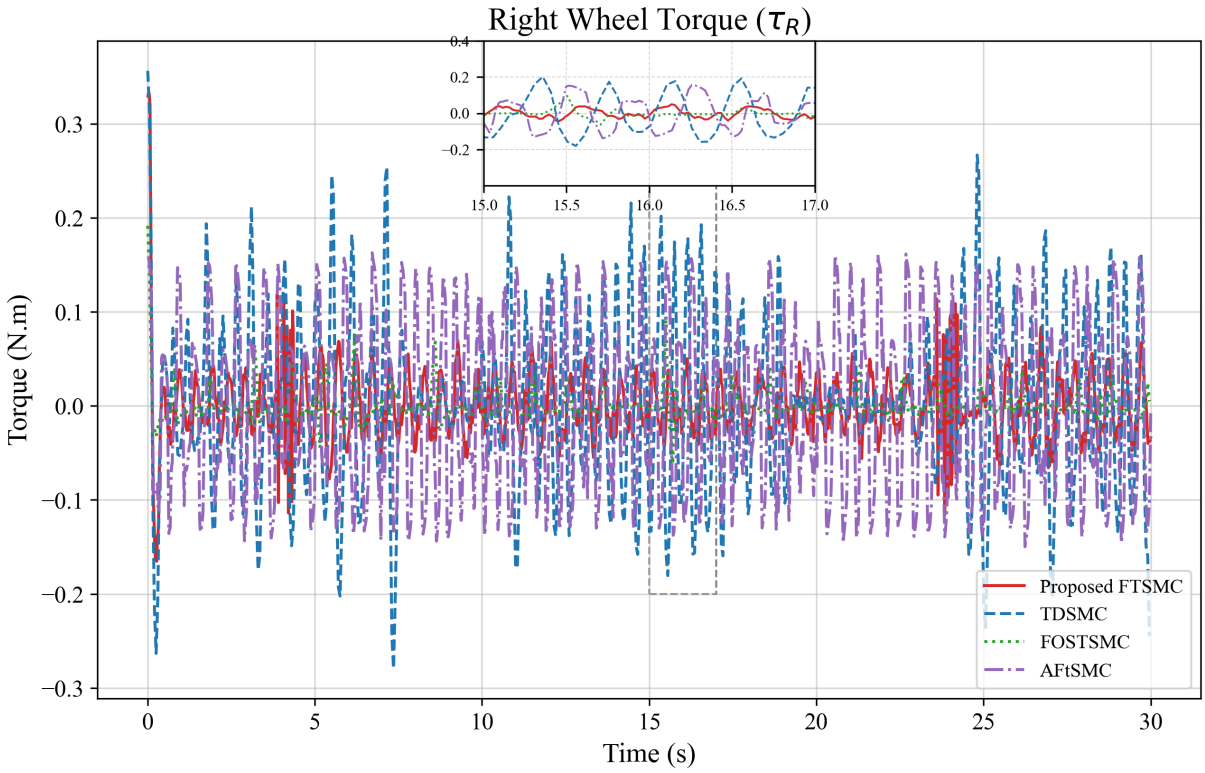


Figure 9. Control input: τ_R without disturbance

7.3.1. Trajectory tracking performance

Figure 10 illustrates the comparative path-tracking capabilities of the three controllers. While all schemes successfully guide the LIMO robot along the reference trajectory, the proposed FTSMC achieves superior performance. Its trajectory aligns almost seamlessly with the target path, even under disturbance. In contrast, TDSMC, FOSTSMC, and AFtSMC exhibit lateral drifting with large tracking errors. Moreover, the simulation of the proposed scheme with different initial values is given in **Figure 11**, which shows that the proposed control method converges within fixed time.

7.3.2. Tracking error analysis

The precision of each method is further quantified by the Cartesian error plots in **Figures 12** and **13**. X-axis: The FTSMC demonstrates the most rapid convergence, forcing the error into a tight neighborhood of zero within a fixed time interval. This proves the controller's ability to maintain a deterministic settling time regardless of initial errors. Y-axis: TDSMC shows poor disturbance rejection, with errors peaking at 14 mm. While FOSTSMC dampens these oscillations, it cannot match the proposed FTSMC, which keeps deviations under 3 mm. This demonstrates the scheme's inherent robustness to impulse and sinusoidal disturbances as defined in our simulation. The proposed FTSMC consistently maintains the Y-axis error below 0.003 m, demonstrating its robustness against unmodeled dynamics and external disturbances.

7.3.3. Velocity tracking analysis

Under the applied disturbances, the commanded and actual velocities of the proposed scheme are depicted in **Figures 14** and **15**. Although the disturbance is injected directly into the velocity dynamics, the actual velocities of the FTSMC remain close to the commands, with only a brief transient excursion at the moment of the impulsive disturbance ($7.0 < t < 7.5$ s). This confirms the disturbance-rejection capability of the discontinuous compensation term $\mathcal{D}\,\mathrm{sign}(s)$ of the proposed control law.

7.3.4. Control input analysis

Efficient control is characterized under disturbance, as shown in **Figures 16** and **17**, where the generated wheel torques for the proposed method are notably smooth.

The proposed FTSMC generates smooth and continuous control signals, effectively mitigating the chattering phenomenon commonly observed in conventional sliding mode controllers. This is attributed to the integral-type sliding surface

and the continuous control law design. In comparison, the control inputs for TDSMC, FOSTSMC, and AFtSMC exhibit higher frequency oscillations, which can lead to mechanical wear and increased power consumption.

7.4. Quantitative comparison

To quantitatively evaluate the tracking performance, the Integral Squared Error (ISE) and Integral Absolute Error (IAE) indices were calculated. The results are summarized in **Table 1**.

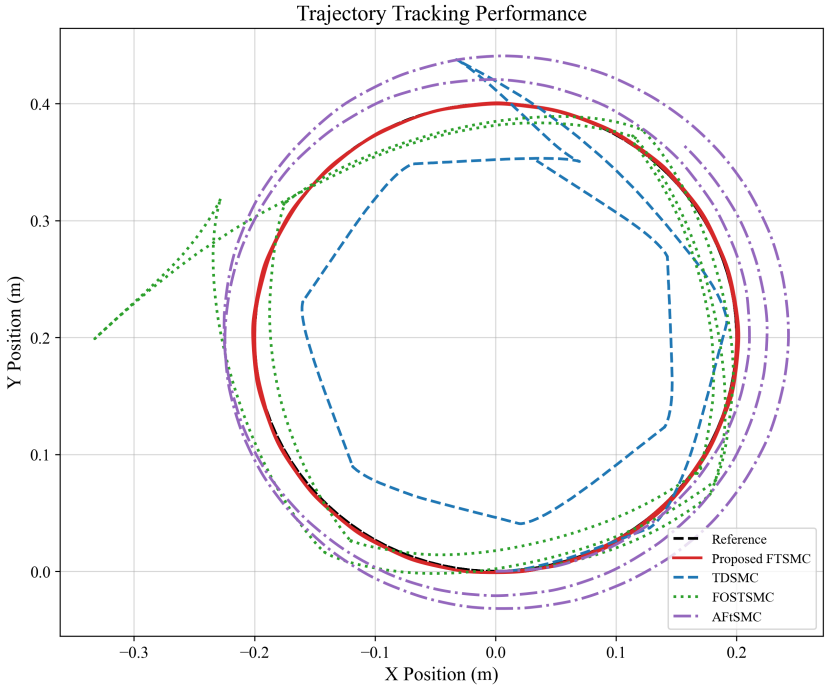


Figure 10. Comparison of trajectory tracking performance in the X-Y plane

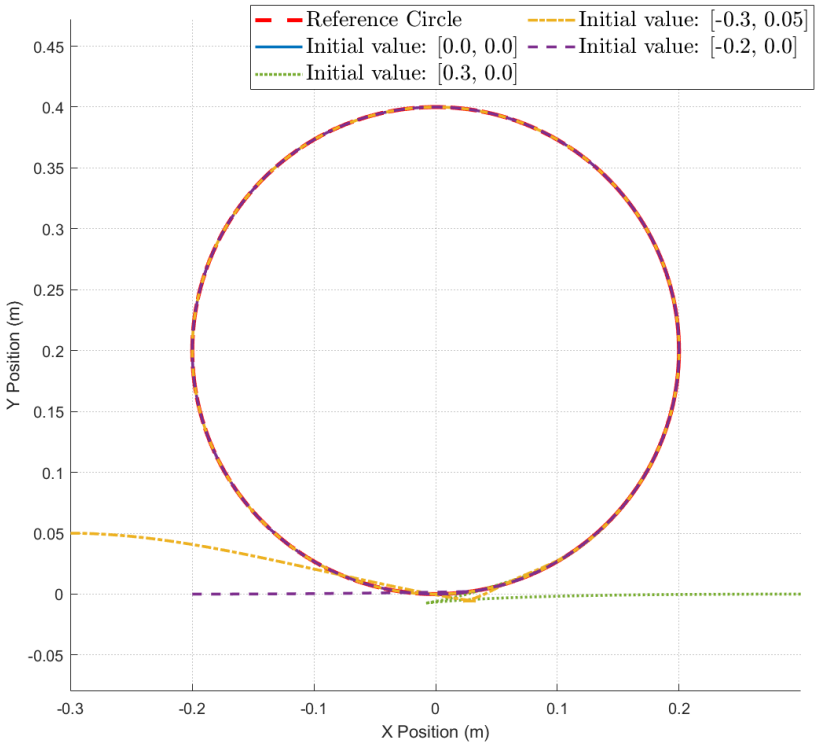


Figure 11. Trajectory tracking performance of the proposed scheme with different initial conditions

The proposed FTSMC achieves the lowest ISE, IAE, and RMSE values among all compared methods, indicating superior precision and faster error convergence. Specifically, the ISE of the proposed controller is reduced by a factor of approximately 1.7, 2.3, and 95 relative to FOSTSMC,

TDSMC, and AFtSMC, respectively. Furthermore, the IAE results indicate that the proposed method reduces the IAE by a factor of approximately 1.3, 1.5, and 9.4 relative to FOSTSMC, TDSMC, and AFtSMC, respectively. The RMSE analysis further substantiates this stability, with the proposed method reducing the RMSE by a factor of approximately 1.3, 1.5, and 9.7 relative to FOSTSMC, TDSMC, and AFtSMC, respectively. These quantitative improvements demonstrate that the proposed fixed-time strategy significantly enhances tracking accuracy and provides greater robustness to system uncertainties than both standard and adaptive sliding-mode approaches.

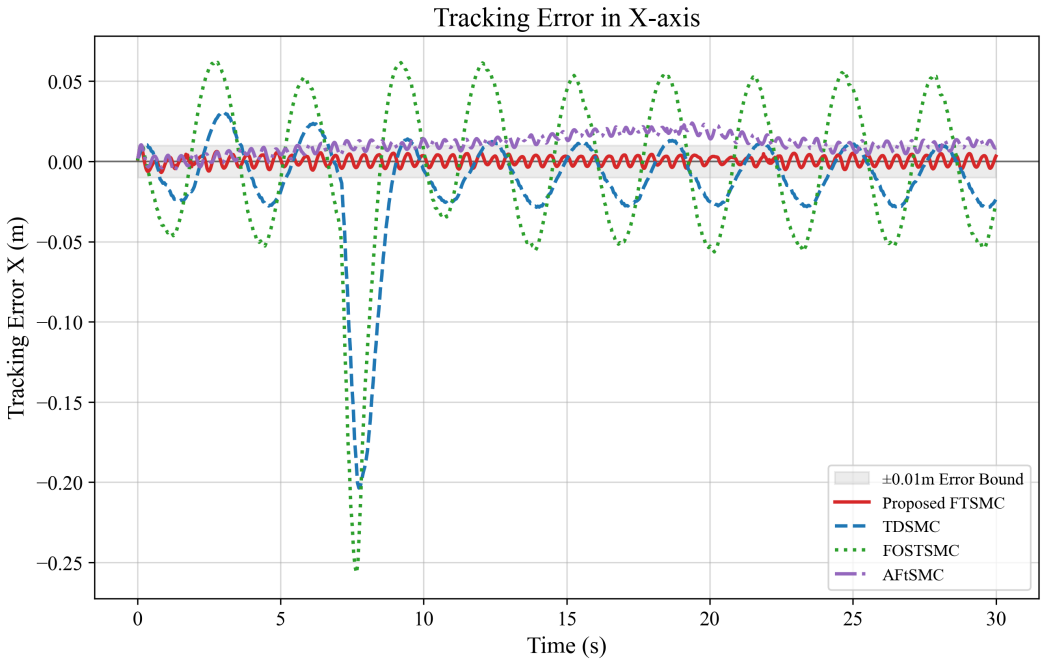


Figure 12. Time evolution of tracking error in X-axis

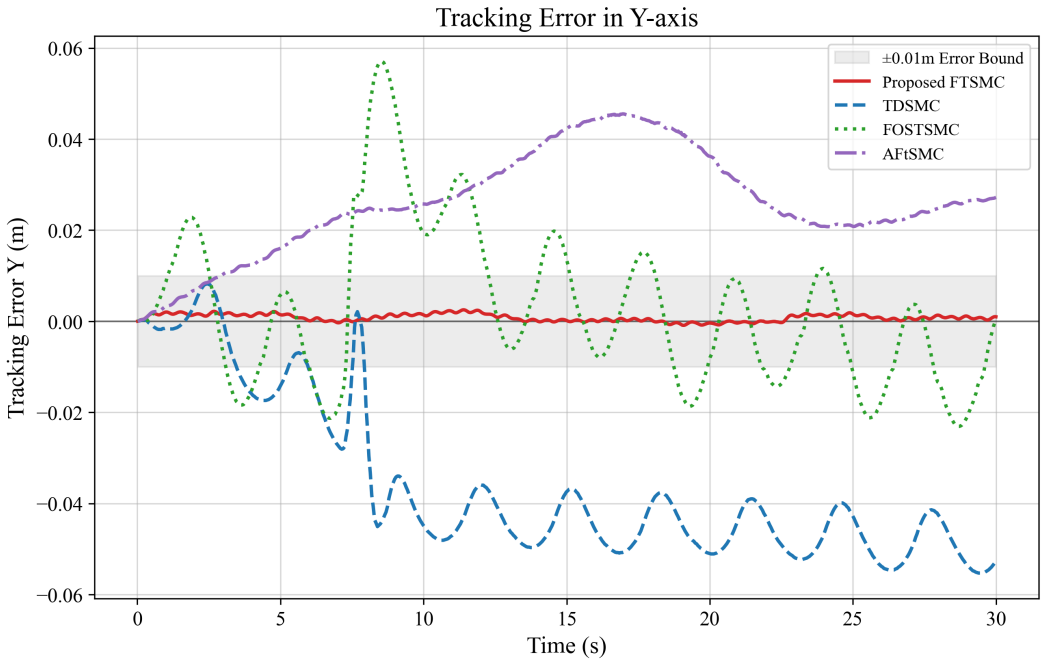


Figure 13. Time evolution of tracking error in Y-axis

To assess the robustness of the proposed technique, **Table 2** presents quantitative performance metrics under disturbances. The results indicate a clear superiority of the proposed FTSMC, which maintains high-precision tracking in the presence of disturbances.

Table 1. Quantitative comparison of tracking performance without disturbance (ISE, IAE, and RMSE)

Controller	**ISE**	**IAE**	**RMSE**
TDSMC	0.0007	0.1353	0.0048
FOSTSMC	0.0005	0.1135	0.0041
AFtSMC	0.0285	0.8512	0.0309
FTSMC	0.0003	0.0902	0.0032

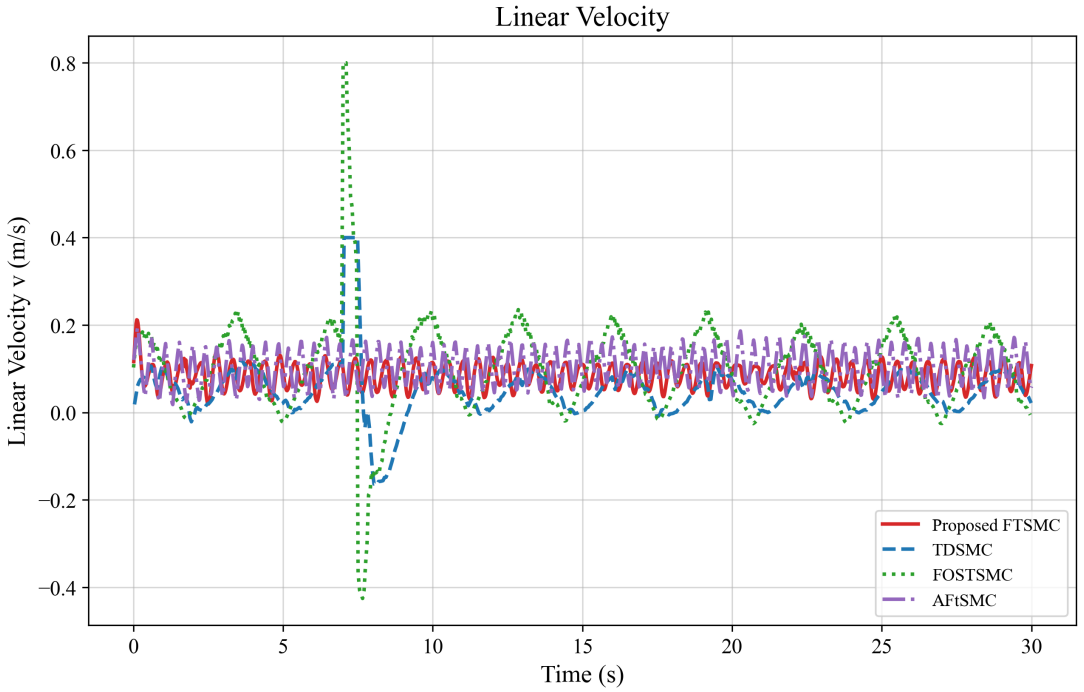


Figure 14. Linear velocity tracking (v_c vs. v) with disturbance

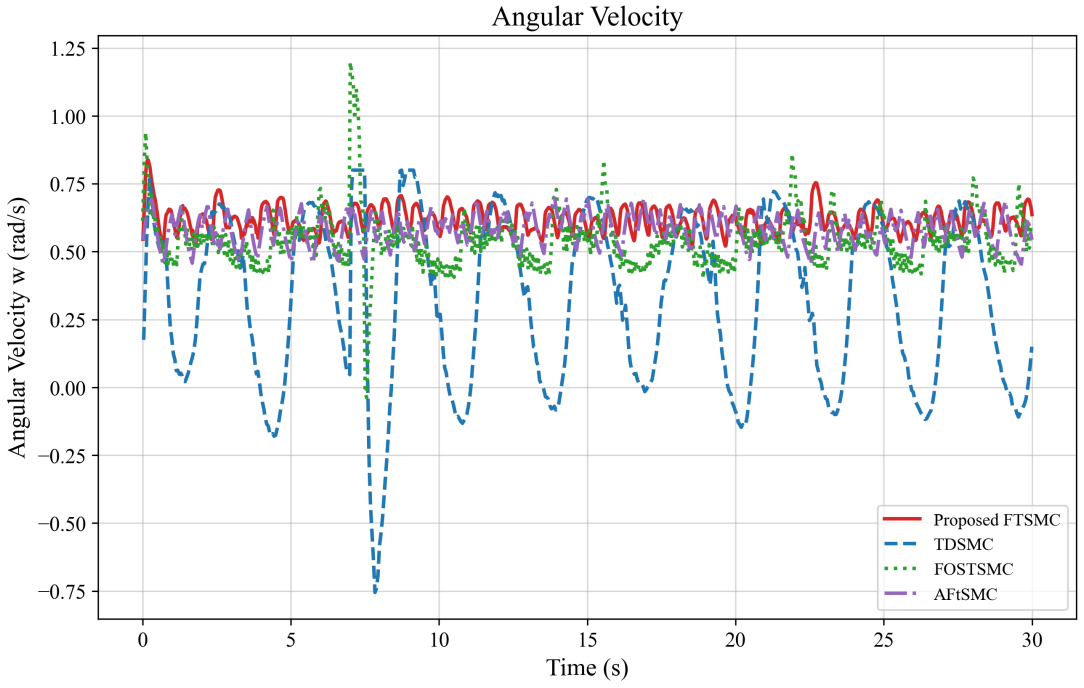


Figure 15. Angular velocity tracking (ω_c vs. ω) with disturbance

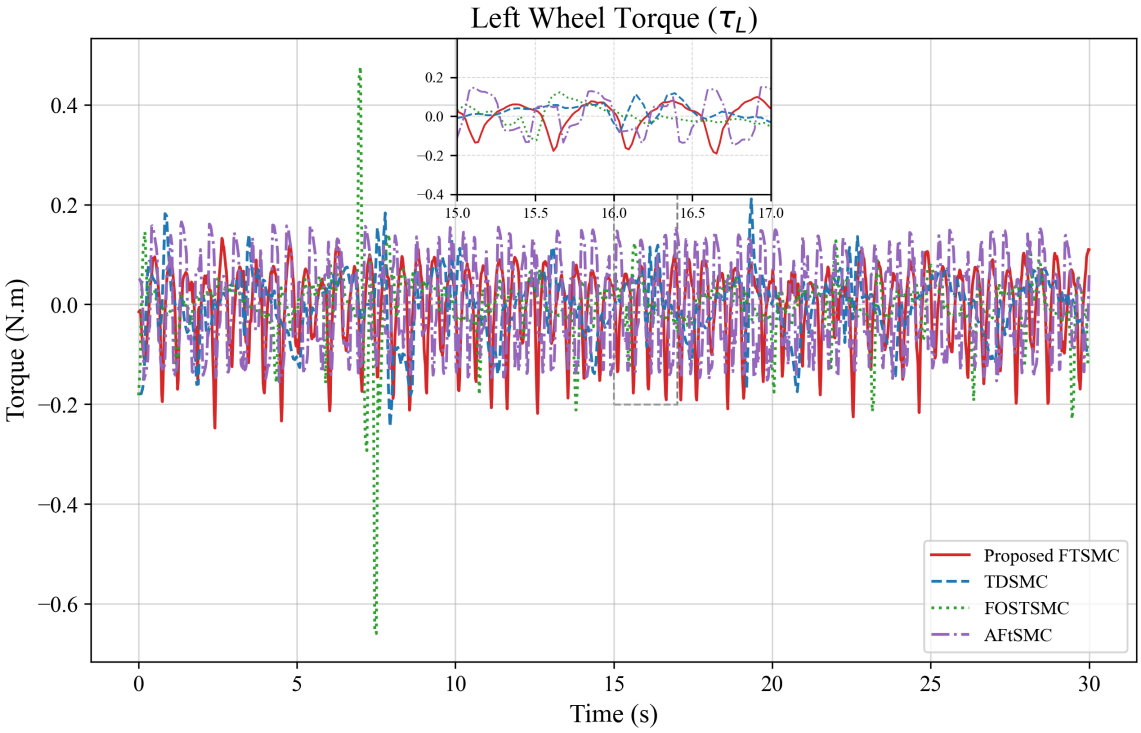


Figure 16. Control input: τ_L with disturbance

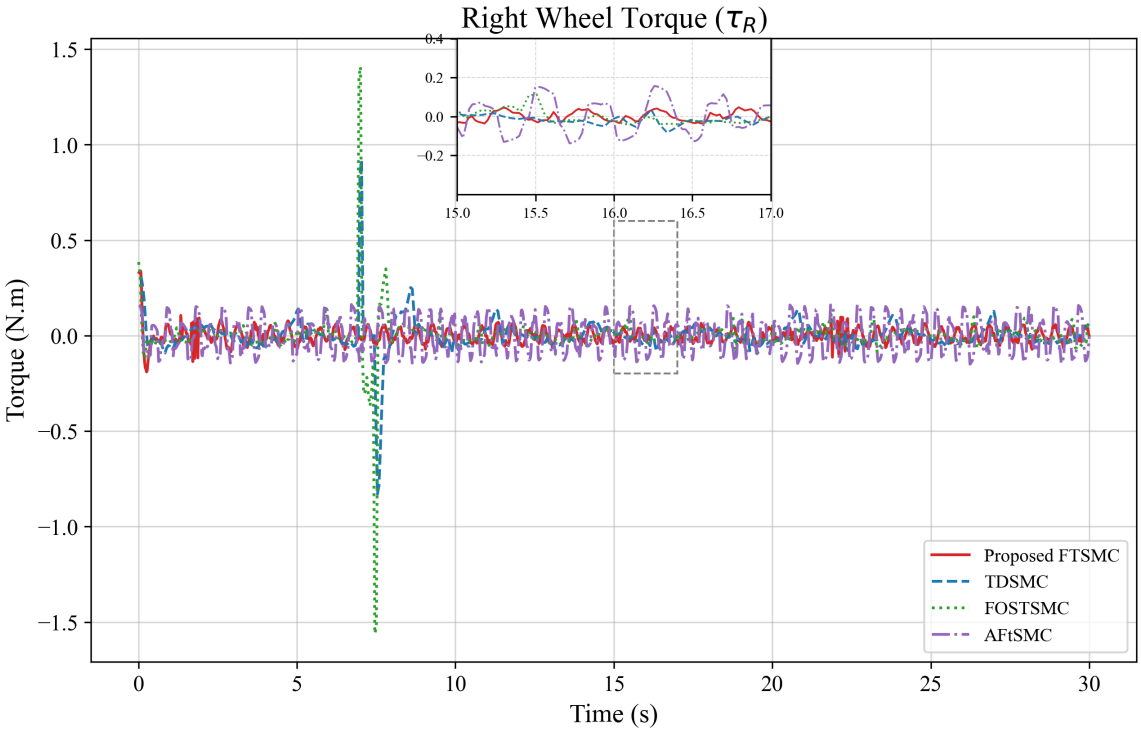


Figure 17. Control input: τ_R with disturbance

Notably, although the tracking errors of all baseline controllers (TDSMC, FOSTSMC, and AFtSMC) escalate considerably during disturbance, the proposed FTSMC sustains an ISE of 0.0003, an IAE of 0.0852, and an RMSE of 0.0032, metrics that are strikingly aligned with the disturbance-free condition. Specifically, the ISE of the proposed controller is reduced by a factor of approximately 286.7, 285, and 107.3 relative to TDSMC, FOSTSMC, and AFtSMC, respectively. Furthermore, the IAE results indicate that the proposed method reduces the IAE by a

factor of approximately 16.2, 15.4, and 11.0 relative to TDSMC, FOSTSMC, and AFtSMC, respectively. The RMSE analysis further substantiates this robustness, with the proposed method reducing the RMSE by a factor of approximately 16.7, 16.7, and 10.3 relative to TDSMC, FOSTSMC, and AFtSMC, respectively. These improvements, attained in the presence of both sinusoidal and impulsive disturbances, demonstrate that the proposed fixed-time strategy preserves its superior precision and robustness under external perturbations.

Table 2. Quantitative comparison of tracking performance with disturbance (ISE, IAE, and RMSE)

Controller	ISE	IAE	RMSE
TDSMC	0.0860	1.3806	0.0535
FOSTSMC	0.0855	1.3102	0.0534
AFtSMC	0.0322	0.9386	0.0328
FTSMC	0.0003	0.0852	0.0032

7.5. Numerical versus experimental validation

To address the consistency between the numerical and experimental results, the tracking behavior of the proposed FTSMC was first evaluated in simulation and then reproduced on the physical platform under the same reference trajectory, controller parameters, and initial conditions. **Figures 18** and **19** report the simulated trajectories of the proposed scheme, confirming the fixed-time convergence property predicted by Theorem 1. In the real-time experiments, the same controller parameters produced the quantitative metrics reported in **Tables 1** and **2**. The experimental ISE and RMSE values obtained in the disturbance-free case (ISE = 0.0003, RMSE = 0.0032) are of the same order of magnitude as the corresponding simulation results, and the small residual differences are attributed to encoder quantization noise, wheel slip, unmodeled friction, and the finite sampling rate of the onboard computer. This consistency between the numerical predictions and the experimental outcomes confirms that the proposed scheme behaves as predicted by the theoretical analysis when deployed on real hardware, thereby experimentally validating the simulation results.

8. Discussion of experimental findings

The experimental findings from the LIMO mobile robot trials confirm the theoretical advantages of the proposed FTSMC scheme compared to existing benchmarks. By examining path-following precision and error dynamics, it is clear that the incorporation of a nonsingular sliding surface with fixed-time stability theory mitigates the inherent constraints of conventional robust control techniques.

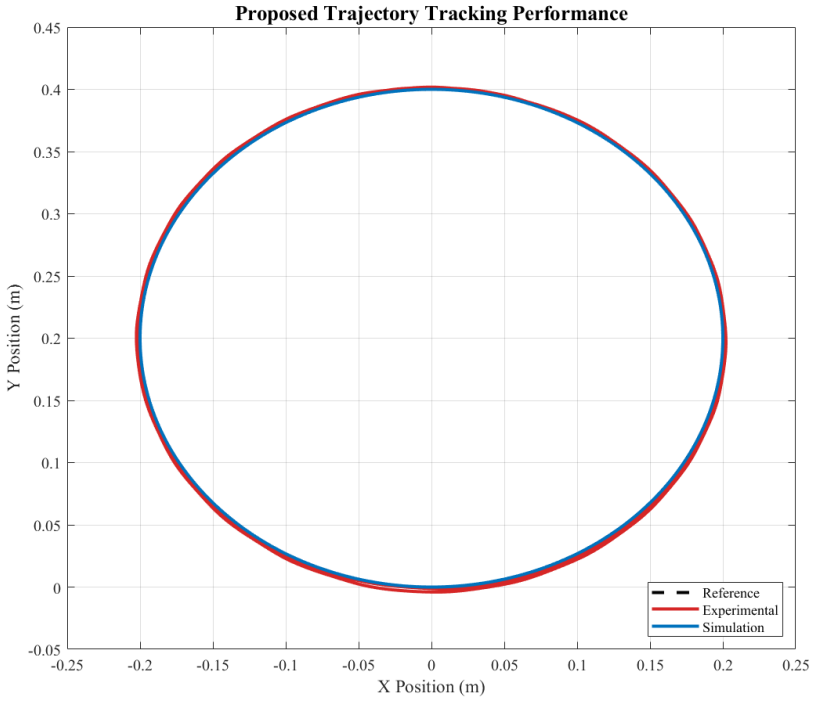


Figure 18. Proposed trajectory tracking performance (simulation and experiment)

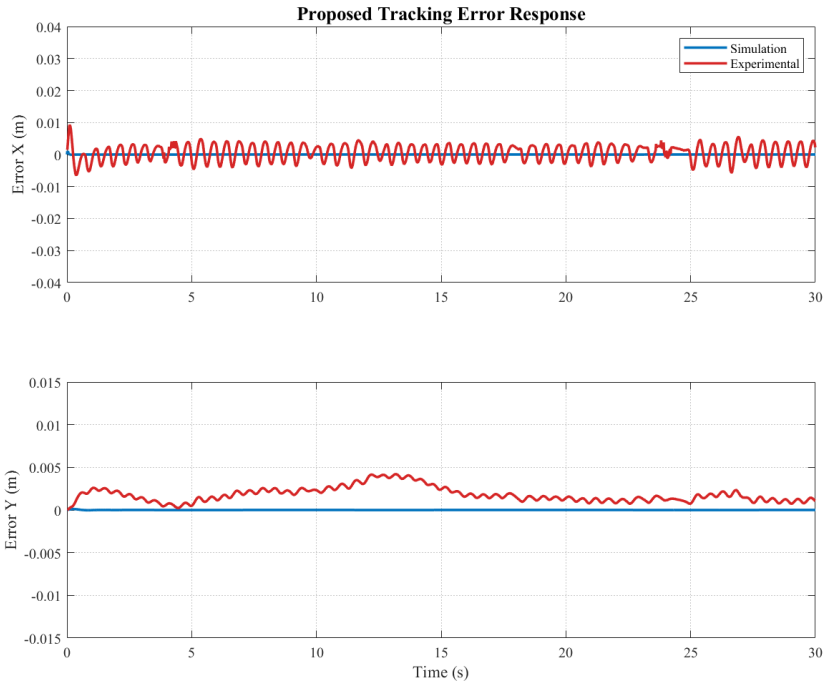


Figure 19. Proposed tracking error performance (simulation and experiment)

8.1. Performance benchmarking and precision

The trajectory tracking performance in the $X-Y$ plane shows a notable difference between the proposed controller and the existing benchmarks. TDSMC, FOSTSMC, and AFtSMC exhibit visible deviations from the reference path, especially during curved sections. The FTSMC, on the other hand, remains quite close to the target coordinates. The Integral Squared Error (ISE) quantifies this improvement. The FTSMC achieved an exceptionally low ISE of 0.0003, which is reduced by a factor of approximately 1.7, 2.3, and 95 relative to FOSTSMC, TDSMC, and AFtSMC, respectively, whereas the IAE and RMSE are reduced by factors of approximately 1.3, 1.5, and 9.4 and 1.3, 1.5, and 9.7 relative to FOSTSMC, TDSMC, and AFtSMC, respectively. The substantial decrease in cumulative error indicates that the proposed law more effectively addresses the nonholonomic constraints and centrifugal forces affecting the LIMO platform during maneuvers. The appropriate parameters for the proposed technique are those chosen in alignment with the specified ranges $k_1, k_2 > 0$, $0 < \alpha < 1$, $\beta > 1$, $K_1, K_2 > 0$, $0 < \bar{\alpha} < 1$, and $\bar{\beta} > 1$. Provided these constraints are respected, the structure of the proposed technique remains unchanged; however, violating them may compromise closed-loop stability. Analysis of the settling-time bounds T_r and T_s reveals an inverse correlation between the gains k_i, K_i and the corresponding settling times, as well as a direct correlation between the gains and the amplitude of the control torque τ. Consequently, increasing k_i and K_i speeds up convergence at the cost of larger control effort, whereas excessively small gains enlarge the settling-time bound. Since the explicit bounds in **Equations (26)** and **(35)** provide the exact relationship between each gain and the guaranteed convergence time, a suitable parameter value can be selected directly from these formulas to meet a prescribed settling-time requirement while respecting actuator limits.

8.2. Advantage of fixed-time stability

A key finding of this research is the nature of the error convergence. Conventional sliding-mode variations frequently rely on asymptotic or finite-time stability, in which the time required for the system to reach the origin is significantly affected by the magnitude of the initial tracking error. In contrast, the proposed FTSMC guarantees that the posture-error system (e_1, e_2, e_3) always reaches the sliding manifold within a bounded time that is independent of the initial posture.

The physical mechanism underlying the proposed fixed-time convergence can be explained as follows. The integral-type sliding surface contains two nonlinear power terms, $k_1 \operatorname{sig}(\bar{e})^{\alpha}$ and $k_2 \operatorname{sig}(\bar{e})^{\beta}$, with $0 < \alpha < 1 < \beta$. For large tracking errors, the term with exponent $\beta > 1$ becomes

increasingly influential and provides strong corrective action, thereby accelerating the reduction of transient error. In contrast, for small tracking errors, the term with exponent $\alpha < 1$ becomes relatively more influential, enhancing convergence toward the origin. Consequently, k_1 and k_2 regulate the convergence strength of the corresponding tracking-error components, while α and β shape the nonlinear convergence characteristics for small and large tracking errors, respectively. Once the sliding motion is established, these terms determine the reduced-order tracking-error dynamics and contribute to fixed-time convergence.

In addition, the reaching law embedded in the control input contains the nonlinear terms $K_1 \operatorname{sig}(s)^{\bar{\alpha}}$ and $K_2 \operatorname{sig}(s)^{\bar{\beta}}$, where $0 < \bar{\alpha} < 1 < \bar{\beta}$. The term associated with $\bar{\beta} > 1$ provides increasingly strong corrective action when the sliding variable s is large, thereby accelerating the initial reaching phase, whereas the term associated with $\bar{\alpha} < 1$ becomes more influential as s approaches zero and enhances the final convergence toward the sliding manifold. Accordingly, K_1 and K_2 regulate the reaching strength, while $\bar{\alpha}$ and $\bar{\beta}$ determine the nonlinear characteristics of the reaching dynamics for small and large values of s, respectively. Increasing these gains generally accelerates convergence but may also increase control effort and sensitivity to measurement noise or actuator limitations; hence, they should be selected to achieve an appropriate trade-off between convergence speed, tracking performance, and control effort. Meanwhile, the explicit disturbance-compensation term $\mathcal{D}\operatorname{sign}(s)$ is introduced to counteract the bounded matched disturbance during the reaching and sliding phases. The combined nonlinear tracking and reaching structures, together with the disturbance compensation, provide the basis for the pre-computable settling-time bounds T_s and T_r established in Theorem 1, thereby guaranteeing fixed-time convergence independently of the initial conditions.

8.3. Actuator health and signal smoothing

One of the most common problems in robust control is the chattering phenomenon, which manifests as high-frequency oscillations in control torques. These oscillations not only reduce tracking accuracy but also accelerate wear on the LIMO's drive mechanism. Our examination of the torque inputs (τ_L, τ_R) indicates that the FTSMC produces smooth and continuous control effort. This result shows that the proposed technique reduces the discontinuous switching common in signum-based controllers. The FTSMC demonstrates that it is a hardware-friendly solution suitable for long-term industrial robotics applications by keeping the Y-axis error below a strict limit of 0.003 m without causing motor vibration. From a practical standpoint, smoother torque signals translate directly into reduced mechanical stress on the gearboxes and lower thermal load on the motor drivers, which prolongs actuator service life and reduces energy consumption over extended operation. This property is particularly relevant for low-cost platforms such as the LIMO robot, whose actuators have limited peak-torque margins and cannot tolerate sustained high-frequency oscillations.

8.4. Implementation feasibility

Finally, the successful implementation of this method on the LIMO's onboard ROS-integrated processor demonstrates its computational efficiency. Even though the mathematical derivation is complex and involves nonlinear reaching principles, the control loop remains lightweight. This makes it possible to integrate FTSMC into existing robotic software stacks without requiring additional high-performance computing hardware. This bridges advanced control theory with real-world robotic applications.

The proposed FTSMC architecture ensures high computational efficiency by utilizing closed-form algebraic operations, achieving a constant $\mathcal{O}(1)$ time complexity with execution times consistently under 1ms. This minimal overhead enables the seamless integration of concurrent high-level tasks, such as trajectory tracking, within a deterministic ROS framework operating at 100Hz (matching the sampling time $T = 0.01$ s used in the experiments). Key tuning parameters, specifically the control gains k_1, k_2, K_1, K_2 and the exponents $\alpha, \beta, \bar{\alpha}, \bar{\beta}$, are calibrated according to the explicit settling-time bounds to optimize the trade-off between convergence speed, chattering attenuation, and control effort. Experimental validation on the LIMO platform confirms that the controller maintains stable, real-time performance and robust disturbance rejection without necessitating iterative re-computation. Such attributes verify the practical feasibility of the algorithm for deployment on resource-constrained mobile robotic systems.

9. Conclusion

Addressing the trajectory tracking requirements of differential-drive LIMO robots under uncertain

operating conditions, this paper proposed a fixed-time sliding mode control strategy utilizing a nonlinear sliding surface. The efficacy of the proposed scheme is demonstrated through experimental implementation; the controller ensures convergence within a predefined time interval while minimizing chattering providing high tracking performance. Quantitatively, in the disturbance-free case the proposed FTSMC reduces the ISE by a factor of approximately 2.3, 1.7, and 95 and the RMSE by a factor of approximately 1.5, 1.3, and 9.7 compared with TDSMC, FOSTSMC, and AFtSMC, respectively. Under the applied disturbances, the proposed scheme attains an ISE that is approximately 286.7 and 285 times smaller than that of TDSMC and FOSTSMC, respectively, and reduces the IAE and RMSE relative to AFtSMC by factors of approximately 11.0 and 10.3, while keeping the Y-axis tracking error below 3 mm. These numerical improvements, together with the smooth wheel torque signals, confirm that the proposed fixed-time scheme outperforms the compared standard and adaptive sliding-mode approaches in both precision and practical applicability. For future work, an adaptive fixed-time SMC scheme will be considered to handle unknown uncertain dynamics and unknown disturbance bounds; the proposed scheme will also be extended to more complex reference paths (e.g., square and Lemniscate/∞-shaped trajectories), to multi-robot formation control built upon the fixed-time framework developed here, and to the integration of disturbance observers for matched and mismatched disturbances.

Acknowledgments

This paper is derived from a research grant funded by the Research, Development, and Innovation Authority (RDIA) - Kingdom of Saudi Arabia, with grant number (13382-psu-2023-PSNU-R-3-1-EI-). The authors would like to thank Prince Sultan University, Riyadh, Saudi Arabia, for supporting the article processing charges (APC) of this publication. The authors especially acknowledge the Automated Systems and Computing Lab (ASCL) at Prince Sultan University, Riyadh, Saudi Arabia.

Funding

This work is funded by Prince Sultan University, Riyadh, Saudi Arabia.

Conflict of interest

The authors declare they have no competing interests.

Author contributions

Conceptualization: All authors
Formal analysis: All authors
Writing-original draft: All authors
Writing-editing & review: All authors

Availability of data

Not applicable.

AI tools statement

During the preparation of this work, the author(s) used an AI assistant in order to assist with drafting and refining the manuscript text and the accompanying software implementation. After using this tool/service, the author(s) reviewed and edited the content as needed and take(s) full responsibility for the content of the published article.

References

1. Moudoud B, Aissaoui H. Fixed-time adaptive sliding mode-based trajectory tracking control for Wheeled Mobile Robot: Theoretical development and real-time implementation. *e-Prime Adv Electr Eng Electron Energy*. 2024;10:100830. https://doi.org/10.1016/j.prime.2024.100830
2. Sun Z, Li Z, Xie H, Zheng Y, Zheng J, Chen B. Precise trajectory tracking of mecanum-wheeled omnidirectional mobile robots via a novel fixed-time sliding mode control approach. *Control Theory Technol*. 2024;22(4):596-611. https://doi.org/10.1007/s11768-024-00224-8
3. Roy S, Nandy S, Ray R, Shome SN. Time delay sliding mode control of nonholonomic wheeled mobile robot: Experimental validation. In: *2014 IEEE International Conference on Robotics and Automation (ICRA)*. IEEE; 2014:2886-2892. https://doi.org/10.1109/ICRA.2014.6907274
4. Moudoud B, Aissaoui H, Diany M. Extended state observer-based finite-time adaptive sliding mode control for wheeled mobile robot. *J Control Decis*. 2022;9(4):465-476. https://doi.org/10.1080/23307706.2021.2024458
5. Mevo BB, Saad MR, Fareh R. Adaptive sliding mode control of wheeled mobile robot with nonlinear model and uncertainties. In: *2018 IEEE Canadian Conference on Electrical & Computer Engineering (CCECE)*. IEEE; 2018:1-5. https://doi.org/10.1109/CCECE.2018.8447570
6. Hameed AH, Al-Samarraie SA, Humaidi AJ. Active unmatched disturbance rejection quasi-sliding observer for electronic throttle valve system based on backstepping control. *SAE Int J Engines*. 2025;18(2):195-211. https://doi.org/10.4271/03-18-02-0011
7. Yavuz M, Öztürk M, Yaşkıran B. Comparison of fractional order sliding mode controllers on robot manipulator. *Int J Optim Control Theor Appl*.

2025;15(2):281.
https://doi.org/10.36922/ijocta.1678

8. Hameed AH, Al-Samarraie SA, Humaidi AJ. Reduced ultimate-bound of tracking error convergence for ETV system with unknown upper-bound mismatched perturbation. *Proc Inst Mech Eng Part D J Automob Eng.* 2025;239(10-11):4952-4971.
https://doi.org/10.1177/09544070241272879
9. Moudoud B, Aissaoui H, Diany M. Adaptive integral-type terminal sliding mode control: Application to trajectory tracking for mobile robot. *Int J Adapt Control Signal Process.* 2023;37(3):603-616.
https://doi.org/10.1002/acs.3540
10. Ma L, Wang C, Ge C, Liu H, Li B. Fixed-time integral sliding mode tracking control of a wheeled mobile robot. *Complex Eng Syst.* 2023;3(10):14.
https://doi.org/10.20517/ces.2023.14
11. Ahmed S, Azar AT. Enhanced tracking control for n-DOF robotic manipulators: A fixed-time terminal sliding mode approach with time delay estimation. *Results Eng.* 2024;24:102904.
https://doi.org/10.1016/j.rineng.2024.102904
12. Sun Y, Gao Y, Zhao Y, et al. Neural network-based tracking control of uncertain robotic systems: Predefined-time nonsingular terminal sliding-mode approach. *IEEE Trans Ind Electron.* 2022;69(10):10510-10520.
https://doi.org/10.1109/TIE.2022.3161810
13. Man Z, Paplinski AP, Wu HR. A robust MIMO terminal sliding mode control scheme for rigid robotic manipulators. *IEEE Trans Autom Control.* 1994;39(12):2464-2469.
https://doi.org/10.1109/9.362847
14. Alnufaie L. Nonsingular fast terminal sliding mode controller for a robotic system: A fuzzy approach. *IEEE Access.* 2023;11:75522-75527.
https://doi.org/10.1109/ACCESS.2023.3288000
15. Zhang Z, Leibold M, Wollherr D. Integral sliding-mode observer-based disturbance estimation for Euler-Lagrangian systems. *IEEE Trans Control Syst Technol.* 2020;28(6):2377-2389.
https://doi.org/10.1109/TCST.2019.2945904
16. Nguyen VC, Kim SH. A novel fixed-time prescribed performance sliding mode control for uncertain wheeled mobile robots. *Sci Rep.* 2025;15(1):5340.
https://doi.org/10.1038/s41598-025-89126-6
17. Sun H, Gao L, Zhao Z, Li B. Adaptive super-twisting fast nonsingular terminal sliding mode control with ESO for high-pressure electro-pneumatic servo valve. *Control Eng Pract.* 2023;134:105483.
https://doi.org/10.1016/j.conengprac.2023.105483
18. Polyakov A. Nonlinear feedback design for fixed-time stabilization of linear control systems. *IEEE Trans Autom Control.* 2012;57:2106-2110.
https://doi.org/10.1109/TAC.2011.2179869
19. Lai Q, Wang J. Finite and fixed-time synchronization of memristive chaotic systems based on sliding mode reaching law. *Acta Phys Sin.* 2024;73(18):180503.
https://doi.org/10.7498/aps.73.20241013
20. Lai Q, Wang J, Huang D. Diverse dynamical behaviors and predefined-time synchronization of a simple memristive chaotic system. *Acta Phys Sin.* 2025;74(20):200501.
https://doi.org/10.7498/aps.74.20250954
21. Lai Q, Wang J, Wang L, Qin M. Fixed-time and predefined-time synchronization of inertial memristive neural networks with proportional delay and mismatched switching jumps via stochastic particle swarm optimization. *IEEE/CAA J Autom Sin.* 2026;13(6):1274-1287.
https://doi.org/10.1109/JAS.2025.126008
22. Sun Y, Liu J, Gao Y, Liu Z, Zhao Y. Adaptive neural tracking control for manipulators with prescribed performance under input saturation. *IEEE/ASME Trans Mechatron.* 2022;28(2):1037-1046.
https://doi.org/10.1109/TMECH.2022.3213441
23. Xu N, Wang T, Niu B, Zong G, Zhao X, Song G. Zero-sum game-based dynamic self-triggered sliding mode control for unknown nonlinear systems with asymmetric input constraints. *ISA Trans.* 2025;168:225-235.
https://doi.org/10.1016/j.isatra.2025.11.014
24. Chu C, He Y. A unified neural event-triggered control approach of high-order switched uncertain systems with time-varying state constraints. *Robot Intell Autom.* 2026;46(3):290-302.
https://doi.org/10.1108/RIA-09-2025-0295
25. Moulay E, Léchappé V, Bernuau E, Defoort M, Plestan F. Fixed-time sliding mode control with mismatched disturbances. *Automatica.* 2022;136:110009.
https://doi.org/10.1016/j.automatica.2021.110009
26. Fang X, Cheng R, Cheng S, Fan Y. Nonsingular fixed-time fault-tolerant sliding mode control of robot manipulator with disturbance observer. *Int J Control Autom Syst.* 2024;22(7):2182-2192.
https://doi.org/10.1007/s12555-022-0594-6
27. Karam ZA, Hassan MY, Humaidi AJ. Unified kinematic-dynamic intelligent formation control via geometric integral sliding mode and IT2 adaptive fuzzy PID controllers for differential-drive mobile robots. *Int J Fuzzy Syst.* 2026:1-21.
https://doi.org/10.1007/s40815-026-02263-6
28. Karam ZA, Hassan MY, Humaidi AJ. Mobile robot formation control based on adaptive-τ Tustin differentiator for estimation of leader velocity. *Int Rev Appl Sci Eng.* 2026;17(2):264-278.
https://doi.org/10.1556/1848.2026.01262
29. Qin M, Dian S, Guo B, Tao X, Zhao T. Fractional-order SMC controller for mobile robot trajectory tracking under actuator fault. *Syst Sci Control Eng.* 2022;10(1):312-324.
https://doi.org/10.1080/21642583.2021.2023683

30. Anjum Z, Chang WJ, Aslam MS, Ullah R. Fixed-time sliding mode control with disturbance observer and variable exponent coefficient for nonlinear systems. *Int J Optim Control Theor Appl.* 2025;15(4):670. https://doi.org/10.36922/IJOCTA025160085
31. Ahmed S, Azar AT. Predefined-time fractional-order terminal SMC for robot dynamics. *Int J Optim Control Theor Appl.* 2025;15(3):426. https://doi.org/10.36922/IJOCTA025060020
32. Moudoud B, Aissaoui H, Diany M. Finite-time adaptive trajectory tracking control based on sliding mode for Wheeled Mobile Robot. In: *2021 18th International Multi-Conference on Systems, Signals & Devices (SSD)*. IEEE; 2021:1148-1153. https://doi.org/10.1109/SSD52085.2021.9429380

Saim Ahmed *received the B. S. degree in Electronics from the Sir Syed University of Science and Technology, Pakistan, in 2009; the M. E. degree in Industrial Control and Automation from Hamdard University, Pakistan, in 2013; and the PhD in Control Science and Engineering from Nanjing University of Science and Technology, China, in 2019. He is currently a Postdoctoral Researcher at the Automated Systems and Computing Laboratory (ASCL), Prince Sultan University, Saudi Arabia. His research interests include the theory and applications of adaptive control, sliding mode control, time-delay control, reinforcement learning, robotic manipulators, mobile robots, biomathematical systems, power systems, and nonlinearities and their compensation.*
https://orcid.org/0000-0002-2302-705X

Zeeshan Haider *is an AI researcher and engineer specializing in machine learning and deep learning, currently focused on large language models, agentic AI, and reinforcement learning. He is a Research Assistant at the Automated Systems and Computing Lab (ASCL) at Prince Sultan University, where he works on multi-agent systems in a joint project with the University of Oxford. He received an M.S. in Artificial Intelligence and Embedded Systems from Information Technology University, Lahore (2019), and a B.S. in Embedded Systems and Electronics from FAST-National University (2017). His research spans reinforcement learning, computer vision, medical image analysis, and natural language processing, with work published in peer-reviewed journals and conferences. He has also built and deployed production AI systems for startups in the USA, Sweden, and Pakistan.*
https://orcid.org/0009-0007-2726-6625

Ahmad Taher Azar *is currently a Full Professor with the College of Computer and Information Sciences (CCIS), Prince Sultan University, Riyadh, Saudi Arabia. He is also the Leader of the Automated Systems and Computing Laboratory (ASCL), Prince Sultan University. He has expertise in artificial intelligence, control theory and applications, robotics, machine learning, computational intelligence, and dynamical system modeling. He has authored/co-authored over 500 research articles in prestigious peer-reviewed journals, book chapters, and conference proceedings. He is an Editor of IEEE Systems Journal, IEEE Transactions on Neural Networks and Learning Systems, Human-Centric Computing and Information Sciences (Springer), and Engineering Applications of Artificial Intelligence (Elsevier).*
https://orcid.org/0000-0002-7869-6373

This work is licensed under a Creative Commons Attribution 4.0 International License. The authors retain ownership of the copyright for their article, but they allow anyone to download, reuse, reprint, modify, distribute, and/or copy articles in IJOCTA, so long as the original authors and source are credited. To see the complete license contents, please visit http://creativecommons.org/licenses/by/4.0/.